

Galaxy populations in the Antlia cluster – III. Properties of faint early-type galaxies[★]

Analía V. Smith Castelli,^{1,2,3†} Sergio A. Cellone,^{1,2,3} Favio R. Faifer,^{1,2,3}
Lilia P. Bassino,^{1,2,3} Tom Richtler,⁴ Gisela A. Romero,^{3,5} Juan Pablo Calderón^{1,2,3}
and Juan Pablo Caso^{1,2,3}

¹Consejo Nacional de Investigaciones Científicas y Técnicas, Rivadavia 1917, C1033AAJ Buenos Aires, Argentina

²Instituto de Astrofísica de La Plata (CCT La Plata, CONICET, UNLP), Paseo del Bosque, B1900FWA La Plata, Argentina

³Facultad de Ciencias Astronómicas y Geofísicas, Universidad Nacional de La Plata, Paseo del Bosque, B1900FWA La Plata, Argentina

⁴Departamento de Astronomía, Universidad de Concepción, Casilla 160-C, Concepción, Chile

⁵Departamento de Física y Astronomía, Universidad de Valparaíso, Avenida Gran Bretaña 1111, Valparaíso, Chile

Accepted 2011 September 27. Received 2011 September 13; in original form 2011 July 26

ABSTRACT

We present a new analysis of the early-type galaxy population in the central region of the Antlia cluster, focusing on the faint systems such as dwarf ellipticals (dEs) and dwarf spheroidals (dSphs). The colour–magnitude relation (CMR) and the relation between luminosity and mean effective surface brightness for galaxies in the central region of Antlia have been previously studied in Paper I of the present series. Now we confirm 22 early-type galaxies as Antlia members, using Gemini-GMOS and Magellan-MIKE spectra. Among them, 15 are dEs from the FS90 Antlia Group catalogue, two belong to the rare type of compact ellipticals (cEs) and five are new faint dwarfs that had never been catalogued before. In addition, we present 16 newly identified low-surface-brightness galaxy candidates, almost half of them displaying morphologies consistent with being Antlia’s counterparts of Local Group dSphs, which extend the faint luminosity limit of our study down to $M_B = -10.1 (B_T = 22.6)$ mag. With these new data, we built an improved CMR in the Washington photometric system, i.e. integrated T_1 magnitudes versus $(C - T_1)$ colours, which extends ~ 4 mag faintwards the limit of spectroscopically confirmed Antlia members. When only confirmed early-type members are considered, this relation extends over 10 mag in luminosity with no apparent change in slope or increase in colour dispersion towards its faint end. The intrinsic colour scatter of the relation is compared with those reported for other clusters of galaxies; we argue that it is likely that the large scatter of the CMR, usually reported at faint magnitudes, is mostly due to photometric errors along with an improper membership/morphological classification. The distinct behaviour of the luminosity versus mean effective surface brightness relation at the bright and faint ends is analysed, while it is confirmed that dE galaxies on the same relation present a very similar effective radius, regardless of their colour. The projected spatial distribution of the member sample confirms the existence of two groups in Antlia, each one dominated by a giant elliptical galaxy and with one cE located close to each giant. Size and position, with respect to massive galaxies, of the dSph candidates are estimated and compared to Local Group counterparts.

Key words: techniques: radial velocities – galaxies: clusters: general – galaxies: clusters: individual: Antlia – galaxies: dwarf – galaxies: elliptical and lenticular, cD – galaxies: photometry.

[★]Based on observations carried out at the Cerro Tololo Inter-American Observatory (Chile), at Las Campanas Observatory (Chile) and at the European Southern Observatory, Paranal (Chile). Also based on observations obtained at the Gemini Observatory, which is operated by the Association of Universities for Research in Astronomy, Inc., under a cooperative agreement with the NSF on behalf of the Gemini partnership: the National Science Foundation (United States), the Science and Technology Facilities Council (United Kingdom), the National Research Council (Canada), CONICYT (Chile), the Australian Research Council (Australia), Ministerio da Ciencia e Tecnologia (Brazil) and Ministerio de Ciencia, Tecnología e Innovación Productiva (Argentina).

†E-mail: asmith@fcaglp.unlp.edu.ar

1 INTRODUCTION

The fact that early-type galaxies in clusters and groups define sequences in the colour–magnitude and surface brightness–luminosity diagrams has been known for a long time (e.g. Baum 1959; Sandage 1972; Kormendy 1977a,b; Visvanathan & Sandage 1977; Sandage & Visvanathan 1978; Caldwell & Bothun 1987; Ferguson & Binggeli 1994). These relations are expected to provide clues about the evolutionary status of the galaxies that follow them and they seem to be universal. Such universality led several authors to suggest their use as reliable distance indicators (e.g. Sandage 1972; Binggeli & Jerjen 1998; Cellone 1999) and to set membership criteria (e.g. Chiboucas & Mateo 2006).

The faint end of these photometric relations is populated by very faint dwarf elliptical (dE) and dwarf spheroidal (dSph) galaxies. Despite morphological criteria have been proved useful for identifying dwarf galaxies in nearby clusters and groups (e.g. Binggeli, Sandage & Tammann 1985; Ferguson 1989; Ferguson & Sandage 1990, hereafter FS90), background galaxies may mimic dwarf morphologies if they are not observed with sufficient spatial resolution (see, for example, object 27 in Conselice, Gallagher & Wyse 2003; Penny & Conselice 2008). This fact may introduce a significant contamination into the observed relations and may cause disagreements in their interpretation. Examples of discrepancies that deserve some analysis are those related with the linearity and the scatter of the colour–magnitude relation (CMR).

Most CMRs show no perceptible change of slope from luminous galaxies to the dwarf regime (Secker, Harris & Plummer 1997; Terlevich et al. 1999; López-Cruz, Barkhouse & Yee 2004; Andreon et al. 2006; Smith Castelli et al. 2008a, hereafter Paper I; Price et al. 2009) except, perhaps, at the very bright end (see fig. 8b in Misgeld, Mieske & Hilker 2008 and fig. 3 in Misgeld, Hilker & Mieske 2009). However, non-linear trends for the CMR of the Virgo cluster have been found (Ferrarese et al. 2006; Janz & Lisker 2009). In addition, there is a considerable increase in the scatter of all CMRs towards their faint end in comparison to that displayed by the brightest galaxies. It is still under discussion whether such increase has a physical origin pointing to differences in ages, metal abundances or formation scenarios among dwarf galaxies (e.g. Conselice, Gallagher & Wyse 2002; Conselice et al. 2003; Penny & Conselice 2008; Jaffé et al. 2011), or whether it can be accounted for by photometric errors (e.g. Secker et al. 1997; Misgeld et al. 2008, 2009; Janz & Lisker 2009) and/or background galaxies contamination (e.g. López-Cruz et al. 2004).

Now, we have spectroscopically confirmed new dwarf Antlia members and we have identified previously non-catalogued dwarf candidates. We revisit the relations analysed in Paper I, i.e. the colour–magnitude and the luminosity–mean effective surface brightness relations, regarding particularly the behaviour of their faint ends. In order to analyse the structure of the Antlia cluster, we study the projected spatial distribution of the whole galaxy sample.

In addition, we have confirmed the existence of two compact elliptical (cE) galaxies in Antlia (Smith Castelli et al. 2008b, hereafter Paper II; Smith Castelli et al. 2009). These are rare low-mass systems; about only a dozen have been identified within a distance of ~ 100 Mpc (Chilingarian & Bergond 2010 and references therein; Huxor et al. 2011) and a similar amount at larger distances (Chilingarian et al. 2009). We include these two peculiar confirmed members in our analysis, thus contributing to the discussion of the alleged dichotomy between bright and faint elliptical galaxies (e.g. Graham & Guzmán 2003; Kormendy et al. 2009; Graham 2011), as cEs are thought to be either the extension to low luminosities of

the family of giant ellipticals (Kormendy et al. 2009 and references therein) or not (Graham 2002).

Finally, physical characteristics of the dSph candidates are compared to galaxies of the same type in other groups and clusters. The dSphs are particularly interesting as they are supposed to be the faintest systems containing dark matter and can be used to constrain cold dark matter (CDM) models of galaxy formation (e.g. Peñarrubia, Navarro & McConnachie 2008, Peñarrubia et al. 2009). Due to their low surface brightness, they have mostly been studied in detail within the Local Group, like the ones surrounding the Milky Way or Andromeda galaxies (e.g. Belokurov et al. 2008; Kalirai et al. 2010).

This paper is based on images of the Cerro Tololo Inter-American Observatory (CTIO) and the Very Large Telescope (VLT), as well as on spectra taken at the Gemini South Observatory and Las Campanas Observatory (LCO). Antlia is the third nearest well populated galaxy cluster after Virgo and Fornax. Before our studies on Antlia (Dirsch, Richtler & Bassino 2003; Bassino, Richtler & Dirsch 2008; Paper I; Paper II), the photographic work of FS90 was the last major effort devoted to study the faint galaxy content in this cluster. They identified, by visual inspection on photographic plates, 375 galaxies in their Antlia Group catalogue down to $M_B = -14.7(B_T = 18)$ mag. Among them, 252 are classified as dwarf galaxies or probable dwarf objects, 71 of which are found in our frames. Only 15 of these 71 galaxies had measured radial velocities at that moment. Our spectra have allowed us to add 23 new radial velocities to this sample (16 early-type and three late-type members plus four background galaxies), and to detect five previously unclassified new Antlia members. In addition, we have visually identified 16 unclassified galaxies displaying dE and dSph morphologies, extending the luminosity range of probable Antlia members down to $M_B = -10.1(B_T = 22.6)$ mag.

Throughout this paper we will adopt $(m - M) = 32.73$ as the Antlia distance modulus (Dirsch et al. 2003). It corresponds to a distance of 35.2 Mpc at which 1 arcsec subtends 170 pc. The paper is organized as follows. Section 2 describes our observational data and Section 3 presents our galaxy sample. In Section 4 we revisit the photometric relations of early-type Antlia galaxies including the newly confirmed members and new dwarf galaxy candidates, and analyse the projected spatial distribution of the whole sample. Section 5 presents a discussion of the results and Section 6 our conclusions.

2 OBSERVATIONAL DATA

We have performed a visual search for new dwarf galaxy candidates on a Kron–Cousins R image obtained with the MOSAIC camera (8 CCDs mosaic imager) mounted at the prime focus of the 4-m Blanco telescope at the CTIO, during 2002 April 4 and 5. This image, as well as a similar one taken in the C band of the Washington photometric system, covers the central region of the Antlia cluster (see Fig. 1). This observational material has already been used in Papers I and II.

One pixel of the MOSAIC camera subtends 0.27 arcsec on the sky. This results in a field of view of 36×36 arcmin² (i.e. about 370×370 kpc² at the Antlia distance). The final R/C images were obtained from the combination of three/seven exposures of 600 s. The seeing full width at half-maximum (FWHM) on these final images is 1 arcsec for the R image and 1.1 arcsec for the C image. R magnitudes were transformed into Washington T_1 magnitudes through the calibration given by Dirsch et al. (2003).

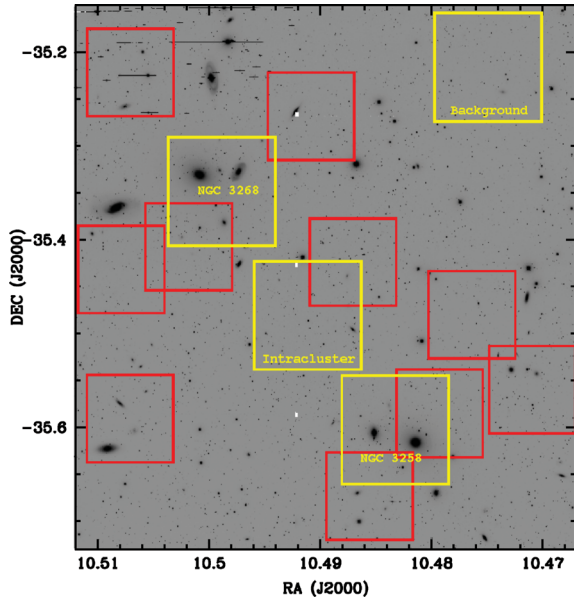


Figure 1. *R* image of the MOSAIC field corresponding to the centre of the Antlia cluster. Yellow squares show the positions of the four FORS1-VLT frames used to check part of our galaxy identifications. Red squares indicate the location of the 10 Gemini-GMOS fields used for spectroscopy (see text). North is up and east is to the left.

Part of our galaxy identification was checked with FORS1-VLT images in the *V* and *I* bands. These images correspond to two fields centred on each of the Antlia dominant galaxies, NGC 3258 and NGC 3268, an *intracluster* field located between both giant galaxies, and a *background* field further away from them (see Fig. 1). We refer to Bassino et al. (2008) for more details on the observations and reduction. In addition, we examined 10 Gemini-GMOS images obtained in the *r*_G0326 filter for designing spectroscopic masks (programs ID: GS-2008A-Q-56, PI: T. Richtler; ID: GS-2009A-Q-25, PI: L. Bassino; ID: GS-2010A-Q-21, PI: L. Bassino). Each image covers a field of view of 5.5×5.5 arcmin² and their scale is 0.146 arcsec pixel⁻¹. The total exposure time of each image is 500 s and the seeing ranges from 0.6 to 0.7 arcsec.

We have also obtained spectra with the Gemini Multi-Object Spectrograph (GMOS) multi-object spectra for the 10 Antlia fields mentioned above (see Fig. 1), from which we measured radial velocities for several galaxies. The B600_G5303 grating blazed at 5000 Å was used with three different central wavelengths (5000, 5050 and 5100 Å) in order to fill in the CCD gaps. A slit width of 1 arcsec was selected; seeing was 0.5–0.6 arcsec in average. This configuration gives a wavelength coverage of 3500–7200 Å depending on the positions of the slits, and a resolution (FWHM) of ~ 4.6 Å. The total exposure times ranged between 2.5 and 3.7 h. Data reduction was performed in a standard manner using the *imred.ccdred.echelle* package within IRAF.¹

In addition, Magellan-MIKE echelle spectra of the two compact elliptical galaxy candidates presented in Paper II (namely, FS90 110 and FS90 192) were obtained at the Clay telescope of Las Campanas Observatory in 2009 March 27 and 28. Slits of 1×5 arcsec and binning 2×3 were used. The spectral coverage at the red

side of the echelle spectrograph was 4900–10 000 Å, with a resolution (FWHM) of ~ 0.35 Å. For FS90 110, two spectra of 900 s and one of 2400 s were obtained, and only one of 2400 s for FS90 192. The reduction was performed using a combination of the IRAF *imred.ccdred.echelle* package, and the *mtools* package written by Jack Baldwin for dealing with the tilted slits in MIKE spectra (available at the LCO website).

Using the Gemini-GMOS spectra, radial velocities were measured with the IRAF task *fxcor* by means of cross-correlation against simple stellar population (SSP) templates suitably selected from the MILES data base (Sánchez-Blázquez et al. 2006). In Table A1 we list the error-weighted average values, and the corresponding errors, obtained for each galaxy with the four templates used ($[Z/H] = -0.71, 0.0$; ages 7.4 and 10.0 Gyr). In the case of galaxies showing bright emission lines, these were used to check and refine the previously measured radial velocities. For the cE galaxy FS90 192, we obtained the radial velocity value by fitting Gaussian profiles with the task *splot* within IRAF, to H α and the Ca II triplet lines.

3 CHARACTERISTICS OF THE GALAXY SAMPLE

3.1 Confirmed Antlia members from the FS90 catalogue

We have obtained new radial velocities for 23 FS90 galaxies. Among them, 20 have become newly confirmed members of the Antlia cluster and three are background galaxies. We recall that we consider as Antlia members all galaxies with radial velocities in the range 1200–4200 km s⁻¹ (see section 2 of Paper I for a justification). In Appendix A we present their coordinates, FS90 morphological classification and membership status as well as the measured radial velocities (Table A1). Logarithmically scaled *R* images of these galaxies are shown in Fig. A1.

We recall that FS90 assigned to each galaxy listed in their Antlia catalogue a membership status: 1 for definite members, 2 for likely members and 3 for possible members. This assignment was based on morphological criteria as only 6 per cent of the listed galaxies had radial velocity determinations at the moment of the catalogue publication.

In general, we confirm the morphological/membership classification assigned by FS90. The exceptions are two cE galaxies (FS90 110 and FS90 192) that are new members of Antlia and were originally considered just as ‘possible’ members, two galaxies originally classified as ‘possible’ and ‘likely’ dE members, which turned out to be an Antlia member (FS90 103) and a background system (FS90 205), respectively, and a confirmed member but with a different (irregular) morphology (FS90 221). As expected, in some objects we are able to see features like nuclei, spiral arms or knots of star formation, thanks to the spatial resolution of our CCD images.

All status 1 galaxies of the spectroscopic sample became confirmed members, while only two of the 20 spectroscopically confirmed Antlia members were classified as status 3 galaxies by FS90 (FS90 110 and FS90 192, the new cE Antlia galaxies). Adding up the 23 FS90 galaxies with new radial velocities presented in this paper with the 37 already presented in Paper I, we have the following statistics: cluster membership is confirmed for 100 per cent (31/31) of FS90 status 1 galaxies, 81 per cent (13/16) of status 2 ones and 54 per cent (7/13) of status 3 objects. This agrees with previous works in the NGC 5044 Group (Cellone & Buzzoni 2005; Mendel et al. 2008), showing that morphologically assigned

¹ IRAF is distributed by the National Optical Astronomy Observatories, which are operated by the Association of Universities for Research in Astronomy, Inc., under cooperative agreement with the National Science Foundation.

memberships are still reliable (mainly for diffuse dwarfs) out to distances of ~ 35 Mpc.

With the addition of the new data, we will revisit the photometric relations of early-type galaxies in the central region of Antlia considering spectroscopically confirmed FS90 members and FS90 galaxies with membership status 1 displaying early-type morphologies. This criterion will allow us to extend the CMR relation down to $M_{T_1} \approx -13$ mag, minimizing contamination by background galaxies lacking radial velocities in this subsample.

We have measured with the task `ELLIPSE` within `IRAF` some galaxies presented with `SEXTRACTOR` (Bertin & Arnouts 1996) photometry in Paper I (see Table C1) in order to compare the measurements obtained with these two softwares (see Appendix C). As bright galaxies were all measured with `ELLIPSE` due to saturation in their central regions (see Paper I for details), we will consider these new photometry in our diagrams and in the different fits performed to the photometric relations.

3.2 New dE members

We have obtained radial velocities for five new Antlia members that were not in the FS90 catalogue. Their radial velocities and photometric parameters are given in Table B1. In Fig. B1 we show the logarithmically scaled R images of these galaxies.

All of them show what seems to be a nucleus. This is a selection effect, as a bright central nucleus turns out to be necessary for obtaining reliable radial velocities from absorption-line spectra of faint diffuse galaxies. Our spectroscopic data include other low-surface-brightness objects without nuclei for which it was not possible to obtain a redshift. Their photometric data were obtained through `SEXTRACTOR` or `ELLIPSE`, depending on whether the object was detected by the former software.

The new members are not catalogued in the NASA/IPAC Extragalactic Database (NED). Therefore, we will refer to them with the acronym `ANTL` followed by the J2000 coordinates, that is `ANTL Jhhmmss–ddmmss`, according to the IAU recommendations for designating new sources (see <http://vizier.u-strasbg.fr/Dic/how.html>).

3.3 New dE and dSph candidates without redshifts

We have performed a visual search on the R MOSAIC image for new dwarf galaxy candidates based on morphological criteria. We looked for extended objects displaying low-surface brightnesses that do not show substructure or evidence of star formation in the C MOSAIC frame. For those objects falling into the deeper FORS and GMOS frames, we have also checked their morphologies by examining their appearance in these deeper images.

As these galaxies are not included in NED, we will designate them in the same way as new dE Antlia members. We present their images in Fig. B2. We obtained integrated magnitudes and colours for all but one of the 16 new dwarf systems (see Table B2). These measurements were performed in the way described in section 2 of Paper I through `SEXTRACTOR` and `ELLIPSE`, or with `PHOT` within `IRAF`. The seven candidates that have no structural parameter determinations are either too faint and diffuse, or are located near bright galaxies or stars which prevented a more exhaustive photometric analysis.

In particular, we are interested in identifying counterparts of Local Group dSph galaxies as they will represent the very faint end of the dwarf galaxy population in Antlia, certainly missed in the FS90 Antlia catalogue. Dwarf spheroidals are low-luminosity ($M_V \gtrsim -13$) galaxies with smooth appearance, which present no evidence of star formation (Kalirai et al. 2010), have low opti-

cal surface brightness ($\mu_V > 22$ mag arcsec $^{-1}$) and no nucleus (Gallagher & Wyse 1994). We have identified 16 galaxies with morphologies consistent with faint early-type galaxies belonging to the cluster. Among them, seven match the dSphs description; they are the ones designated with order numbers 4, 8, 12, 13, 14, 15 and 16 in Table B2.

4 RESULTS

4.1 Colour–magnitude relation

In Fig. 2 we show the CMR defined by FS90 early-type galaxies that are spectroscopically confirmed Antlia members or were considered as definite members (status 1) in the FS90 Antlia catalogue. We have added the new dwarf galaxies presented in the previous section. Several biweight fits to the observed relation have been performed, some of them considering only spectroscopically confirmed members (see Table 1). Following Grebel (2005), we will consider as dwarf galaxies those with $M_V \sim -18$ mag, which corresponds to $T_1 > 14$ mag at the Antlia distance (see table 3a from Fukugita, Shimasaku & Ichikawa 1995). In order to test the results found by Barazza et al. (2009) in Abell 901/902 regarding the existence of a colour–density relation in the projected radial distribution, we divided our dwarf galaxy sample into systems displaying redder and bluer colours than the mean CMR.

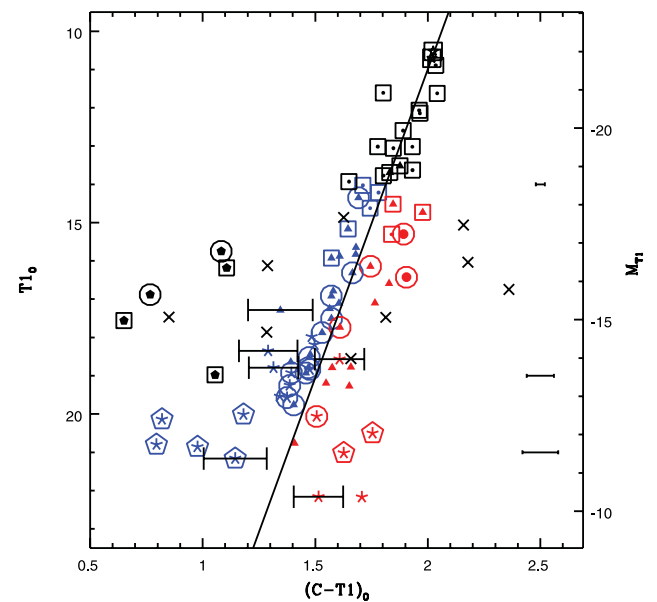


Figure 2. Reddening and extinction-corrected colour–magnitude diagram for FS90 Antlia definite and confirmed members plus new dwarf galaxy candidates and members. Big stars: Antlia’s giant ellipticals; filled circles: cEs; filled triangles: ellipticals; dots: S0s; filled pentagons: dIs and BCDs; asterisks: new dwarf candidates, with those displaying dSph morphologies within open pentagons; open squares: Antlia confirmed members from Paper I; open circles: confirmed members from Gemini and Magellan data. The solid line shows the fit to all early-type galaxies in the sample. We have also plotted the location of FS90 confirmed background galaxies (crosses) in order to see the scatter introduced by these objects to the relation. The isolated error bars show typical colour errors corresponding to the range $10 < T_1 < 18$ (small, 0.02 mag), $18 < T_1 < 20$ (medium, 0.06 mag) and $20 < T_1 < 22$ (large, 0.08 mag). For clarity, we only show individual error bars for those objects with colour uncertainties larger than 0.1 mag. Red and blue symbols depict dwarf galaxies showing redder and bluer colours than the mean CMR, respectively.

Table 1. Results of least-square biweight fits $T_{10} = a + b(C - T_1)_0$ performed to the absorption and extinction-corrected CMR of early-type definite members of Antlia (i.e. FS90 early-type status 1 objects and early-type galaxies with radial velocities). The first column indicates the different samples and the second column gives the number of data points. Slopes and zero-points given in the third and four columns correspond to reddening and extinction-corrected mean CMRs. In the fifth column we show the observed scatter around the mean relation for each sample. In the sixth column we indicate the corresponding mean colour error (ϵ). Following Terlevich, Caldwell & Bower (2001, see their equation 1), we calculate the intrinsic scatter, given in the last column, as $\sigma_{\text{intr}} = \sqrt{\sigma_{\text{obs}}^2 - \langle \epsilon \rangle^2}$. The limiting magnitude adopted to separate bright and dwarf galaxies ($T_1 = 14$ mag) corresponds to $M_V \sim -18$ mag (Grebel 2005).

Sample	Data	a	b	$\sigma_{(C-T_1)_0}$ observed	$\langle \epsilon_{(C-T_1)_0} \rangle$	$\sigma_{(C-T_1)_0}$ intrinsic
All definite+confirmed members	58	43.2 ± 2.7	-16.1 ± 1.5	0.10	0.03	0.09
Dwarf definite+confirmed members	43	44.7 ± 5.7	-17.0 ± 3.5	0.11	0.04	0.10
E definite+confirmed members	42	41.6 ± 3.3	-15.1 ± 1.9	0.10	0.04	0.09
All confirmed members	42	43.0 ± 3.4	-16.0 ± 1.9	0.09	0.03	0.08
Bright confirmed members	15	44.5 ± 10.4	-16.7 ± 4.8	0.06	0.02	0.06
Dwarf confirmed members	27	43.6 ± 8.0	-16.4 ± 4.3	0.10	0.03	0.09
Dwarf confirmed members no cEs	25	42.2 ± 5.9	-15.8 ± 3.3	0.08	0.03	0.07
E confirmed members	26	41.2 ± 4.2	-14.8 ± 2.3	0.09	0.03	0.08
E confirmed members no cEs	24	39.7 ± 2.9	-14.2 ± 1.6	0.07	0.03	0.06
S0 confirmed members	16	40.4 ± 8.5	-14.7 ± 4.1	0.08	0.02	0.07

From Fig. 2 and Table 1, we can see that spectroscopically confirmed members define a tight relation down to $T_{10} = 20$ mag with no change of slope or increase in the scatter. The new dwarf galaxy candidates seem to extend the relation down to $T_{10} > 22$ mag, although introducing a considerable dispersion in the CMR at its very faint end. In particular, dSph candidates tend to increase the scatter towards bluer colours than the mean relation. In comparison with the results presented in Paper I, the CMR gets slightly steeper with the addition of the newly confirmed members. When FS90 non-confirmed members are included in the fit, both the slope of the CMR and its scatter increase.

The selection of the spectroscopic targets was performed independently of their location in the photometric relations analysed in this paper. The Gemini-GMOS fields were chosen to include as many FS90 galaxy candidates as possible. Therefore, it is remarkable that all early-type confirmed members suite so well in the CMR. In addition, we can see that spectroscopically confirmed background galaxies included in the FS90 Antlia catalogue, as well as dI and BCD confirmed members, would introduce a substantial dispersion to the relation if they were wrongly considered as early-type cluster members.

The newly confirmed cE galaxies share the same CMR as ‘normal’ early-type dwarf galaxies. However, as can be seen from the data included in Table 1, they increase the dispersion of the relation defined by dwarf confirmed members towards the red side of the colour–magnitude diagram. When these peculiar galaxies are excluded from the fit, faint early-type members define a CMR with a similar scatter to that traced by bright ones. The location of both cEs in the CMR diagram is consistent with a luminosity fading (≈ 2.8 mag for FS90 110 and ≈ 3.7 mag for FS90 192) at constant colour.

4.2 Surface brightness–luminosity relation

In Fig. 3 we present the revised luminosity– $\langle \mu_{\text{eff}} \rangle$ relation of FS90 Antlia definite and confirmed members, and new dwarf candidates and members. We show, as a dashed line, the locus of constant effective radius ($r_{\text{eff}} \sim 1$ kpc) found for galaxies fainter than $T_{10} = 13$ mag in Paper I. Recall that lines parallel to this locus to-

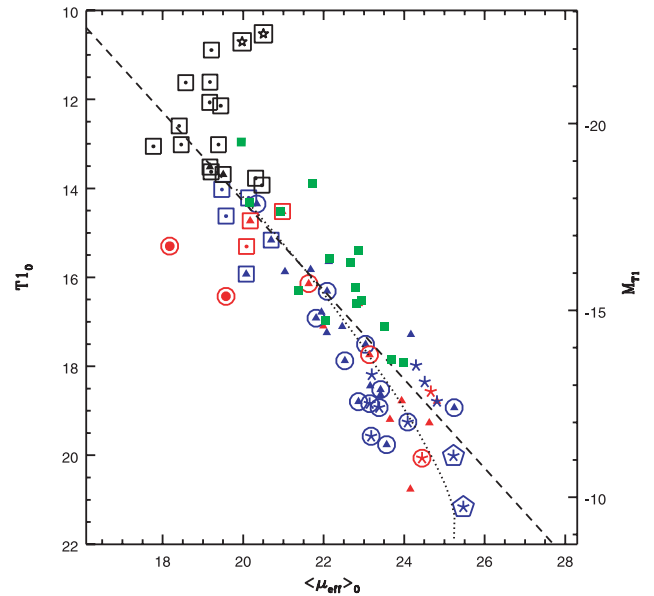


Figure 3. Extinction-corrected T_1 magnitude versus mean effective surface brightness diagram for Antlia definite and confirmed members plus new dwarf galaxy candidates and members. The dashed line shows the locus of constant effective radius (~ 1 kpc) followed by FS90 galaxies fainter than $T_1 = 13$ mag (Paper I). New dwarf galaxy candidates tend to depart towards smaller r_{eff} . The dotted line shows the theoretical effect of isophotal truncation (at 26.0 mag arcsec $^{-2}$) on the galaxy surface brightness distributions at the faint end of the relation. The symbol code for Antlia galaxies is the same as in Fig. 2. Red and blue symbols depict dwarf galaxies showing redder and bluer colours than the mean CMR, respectively. Green squares represent the early-type population of poor groups recently studied by Annibali et al. (2011).

wards fainter luminosities correspond to smaller effective radii (see equation 1 in Paper I).

For our new sample of dwarf early-type members and candidates, we obtain a mean effective radius of $\langle r_{\text{eff}} \rangle = 0.81$ (rms 0.31) kpc, considering 57 galaxies with $T_{10} > 13$ mag and excluding the two

cEs which represent extreme cases. However, we see that both FS90 and newly confirmed members fainter than $T_{10} \sim 18$ mag tend to depart from the linear relation towards smaller effective radii. When only dwarf galaxies in the range $13 < T_{10} < 18$ are considered, the mean effective radius increases to $\langle r_{\text{eff}} \rangle = 0.93$ (rms 0.28) kpc.

One possible explanation for the faint break is that it arises due to the isophotal limit of our photometry, which causes different fractions of galaxy luminosity to be lost outside the limiting isophote for galaxies with different profile shapes. In order to quantify this effect, we considered a set of Sérsic models spanning an appropriate magnitude range, with shape parameters (n) following the luminosity–shape relation given by Graham & Guzmán (2003, see their fig. 10). We fixed the effective radii of all the models at 1 kpc (5.87 arcsec at the Antlia cluster distance), and we then computed for each model the fraction of light lost outside the limiting radius, and the effective radius ‘measured’ from the truncated profile (see Trujillo, Graham & Caon 2001 for the relevant expressions). We thus obtained for each model the values of isophotal magnitude and mean effective surface brightness that would be measured from a truncated profile.

We show the results in Fig. 3, where the dotted line follows the isophotal magnitude versus mean effective surface brightness relations for Sérsic models truncated at isophotal radii corresponding to 26.0 mag arcsec $^{-2}$. While profile truncation always leads to a magnitude dimming and a lower measured r_{eff} , low n (i.e. fainter) galaxies are more strongly affected than galaxies with $n \geq 1$. This gives a curved relation in the observed magnitude versus mean effective surface brightness plane, which should be a straight line for galaxies with the same effective radius. Then, the downturn of the relation for our dwarfs at faint galaxy magnitudes may be attributed to this effect, corresponding to our limiting isophote of about 26.0 mag arcsec $^{-2}$. The same departure towards fainter magnitudes of the dwarfs at the faint end of this relation, with respect to the general trend, is present in the compilation from different environments by De Rijcke et al. (2009).

Both cE galaxies clearly depart from the locus of constant effective radius but, at first glance, in a different manner. FS90 110 seems to extend the break defined by the brightest galaxies towards fainter magnitudes, but FS90 192 is located with the bulk of early-type dwarf galaxies defining what could be their low-limiting r_{eff} . If we calculate for their luminosities the corresponding $\langle \mu_{\text{eff}} \rangle$ on the locus of $r_{\text{eff}} = 1$ kpc, we obtain that they differ from the measured values in $\Delta \langle \mu_{\text{eff}} \rangle = 2.9$ mag arcsec $^{-2}$ for FS90 110, and $\Delta \langle \mu_{\text{eff}} \rangle = 2.7$ mag arcsec $^{-2}$ for FS90 192. Therefore, both cE galaxies depart from the trend defined by early-type dwarf galaxies in a similar manner, defining what could be a photometric criterion to identify candidate cE galaxies. Alternatively, the location of the cEs with respect to the surface brightness–luminosity relation can be judged as consistent with a stripping scenario.

The luminosity–effective radius diagram presented by Barazza et al. (2009) in Abell 901/902 (their fig. 2a) shows that their galaxies scatter about a mean constant effective radius. In Fig. 3, the galaxies located below the dashed line have $r_{\text{eff}} < 1$ kpc and those found above the line, $r_{\text{eff}} > 1$. We see that early-type dwarfs in the central region of Antlia, either redder or bluer than the colour of the mean CMR, show similar effective radii, in agreement with Barazza et al.’s findings. In particular, red dwarfs (excluding the two cEs, 16 galaxies) display a mean effective radius $\langle r_{\text{eff}} \rangle = 0.74$ (rms 0.34) kpc, while blue dwarfs (33 systems), $\langle r_{\text{eff}} \rangle = 0.79$ (rms 0.30) kpc.

We have also plotted, with green squares, the data corresponding to the study of the early-type galaxy population in poor groups performed by Annibali et al. (2011). The bright and faint early-

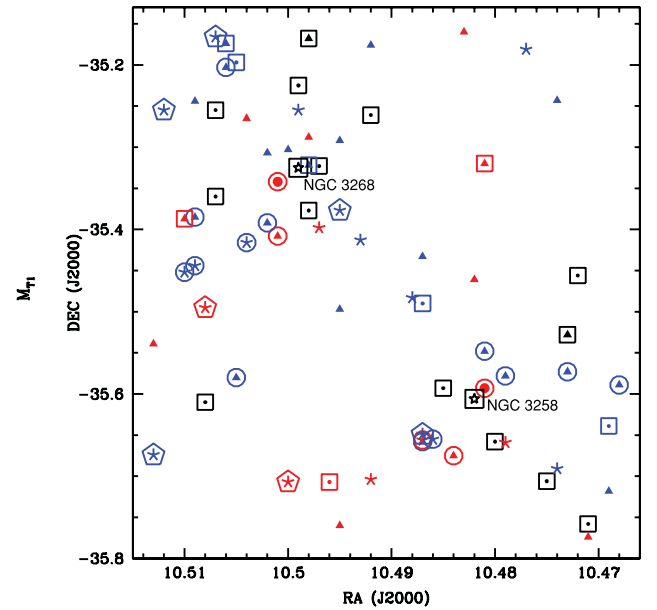


Figure 4. Distribution of the galaxy sample in the MOSAIC field. The symbol code is the same as in Fig. 2. Red and blue symbols depict dwarf galaxies displaying redder and bluer colours than the mean CMR, respectively. North is up and east is to the left.

type systems in these groups follow the luminosity– $\langle \mu_{\text{eff}} \rangle$ relation defined by the Antlia galaxies.

4.3 Projected spatial distribution

In Fig. 4 we show the location of our galaxy sample in the MOSAIC field. Two concentrations of galaxies are present around NGC 3258 and NGC 3268, respectively, with a poorly populated zone between them. Both concentrations are similar in number of galaxies, contain several bright lenticulars, and in each of them there is a cE galaxy placed in the neighbourhood of the dominant system.

Barazza et al. (2009) have shown that redder dwarf early-type galaxies in Abell 901/902 are located closer to the central cluster galaxies than bluer ones of similar luminosity. In our case the mean distances of the dwarfs to each one of the two dominant galaxies (the closer one) are 8.0 (rms 4.8) arcmin for the 20 dwarfs redder than the mean CMR at the same luminosity and 7.7 (rms 4.3) arcmin for 37 dwarfs bluer than the mean CMR. If we consider the luminosity ranges $14 < T_{10} < 17$, $17 < T_{10} < 20$ and $T_{10} > 20$, we obtain, respectively, mean distances of 8.2 (rms 6.1) arcmin (7 red dwarfs) and 8.4 (rms 4.8) arcmin (12 blue dwarfs), 8.3 (rms 5.6) arcmin (7 red dwarfs) and 7.6 (rms 4.5) arcmin (20 blue dwarfs), and 7.4 (rms 2.0) arcmin (6 red dwarfs) and 5.9 (rms 1.1) arcmin (5 blue dwarfs). Therefore, we do not find a clear trend in the sense of that reported by Barazza et al. However, these differences are rather marginal and should be tested with a larger sample including the outer regions of Antlia.

5 DISCUSSION

5.1 Colour–magnitude relation

5.1.1 Interpretation

The CMR of early-type galaxies in groups and clusters of galaxies is a well-known photometric relation that has been studied for long.

In the colour–magnitude diagram, early-type galaxies define a sequence in the sense that bright galaxies are redder than fainter ones. The physical interpretation of this feature has been the subject of numerous observational and theoretical studies. While luminosity or brightness can be easily associated with the (stellar) mass of a galaxy, the well-known *age–metallicity* degeneracy prevents a clear physical identification for integrated colours.

From the study of photometric indices correlated with line strengths for 31 elliptical galaxies belonging to pairs or small groups, Faber (1973) has found that, for the redder galaxies of the sample, the differences in integrated colours are correlated with variations in abundances. In a more recent work, Terlevich et al. (1999) have studied the C_24668 , $Fe4383$, $H\gamma_A$ and $H\delta_A$ spectral absorption line indices of 101 galaxies in the Coma cluster. They found that the CMR in Coma is mainly driven by a luminosity–metallicity effect. This is consistent with the results of Trager et al. (2000) about Fornax and Virgo elliptical galaxies. They are basically old stellar systems and define a mass–metallicity trend, in contrast with field ellipticals, where age and α -element fraction may be more strongly correlated with stellar mass than overall metallicity. This finding for field galaxies is confirmed by Howell (2005); however, his sample covers a small luminosity range which strongly limits any analysis of correlations involving absolute magnitudes.

Clemens et al. (2011) show the mid-infrared CMR for early-type galaxies in the Virgo cluster with absolute K -band magnitudes between -26 and -19 . By comparing their results with those of optical studies, they conclude that the CMR is driven by metallicity effects, as a mass–age relation would produce a slope in the opposite sense to that observed. Observations of clusters at intermediate redshift showed that the slope of the CMR display small variations with redshift (Jaffé et al. 2011, and references therein).

Hence, although other stellar population parameters such as age and α -element fraction are shown to depend on the luminosity of early-type galaxies, and this behaviour is shown to depend on the environment, a clear mass–metallicity relation holds through different environments, from rich clusters to the Local Group, spanning more than five decades in $\log(M_*)$ (e.g. Mendel et al. 2009).

Within the discussion of the CMR in Antlia, it may be thus interesting to turn, as a comparison, to the NGC 5044 group, a relaxed galaxy aggregate intermediate between small groups and rich clusters (Forbes 2007), where early-type galaxies are also found to follow a well-defined CMR spanning ~ 10 mag in luminosity (Cellone & Buzzoni 2005). A spectroscopic analysis relying on Lick indices (Mendel et al. 2009) shows that, among different stellar population parameters, metallicity displays the strongest correlation with stellar mass. There is, however, a clear decoupling between Fe and the α -elements (mostly traced by Mg and Ca) which extends down to the dE mass range (see also Buzzoni et al. 2011). This behaviour confirms and extends previous results which point at different enrichment channels acting along the mass sequence of early-type galaxies in groups and clusters, as a consequence of different star formation efficiencies taking place at different masses. Age effects, although playing a minor role, are certainly present, as witnessed by a small number of ‘blue-nucleus’ dEs with Balmer emission lines in their spectra (e.g. Cellone & Buzzoni 2001; Lisker et al. 2006).

At the lowest stellar-mass extreme, it is expected that dSphs, such as their Local Group counterparts, have experienced complex star

formation histories (e.g. Tolstoy, Hill & Tosi 2009 and references therein). A low metal content is, however, their general characteristic, and should be the main driver of their optical integrated colours.

Therefore, despite the identification of the physical mechanisms involved in defining the CMR is still an open issue, there is strong evidence that the CMR should be mainly interpreted as a mass–metallicity relation.

5.1.2 Observed characteristics

It is widely accepted that the CMR is linear along its extension, and that it shows no perceptible change of slope from the bright galaxies to the dwarf regime (Secker et al. 1997; Terlevich et al. 2001; López-Cruz et al. 2004; Andreon et al. 2006; Paper I; Misgeld et al. 2008, 2009). In addition, there is strong evidence for the universality of this relation in clusters of galaxies.

Bower, Lucey & Ellis (1992) have found that early-type galaxies in Virgo and Coma present *identical* ($U - V$) and ($V - K$) colours, following the same linear CMR. Conselice et al. (2002) found, for the Perseus cluster, a fit to the bright end of the CMR in agreement to that derived by Secker et al. (1997) for the Coma cluster. In Paper I we have obtained a linear fit to the CMR of the Antlia cluster with a slope in agreement with those found for dwarf galaxies in Virgo (Lisker, Grebel & Binggeli 2008), Fornax (Hilker, Mieske & Infante 2003; Mieske et al. 2007), Perseus (Conselice et al. 2002) and Coma (López-Cruz et al. 2004). De Rijcke et al. (2009) have shown that early-type galaxies belonging to different clusters and groups do follow the same colour–magnitude relation. Moreover, in Perseus (Penny et al. 2011) and Coma (Terlevich et al. 2001) it has been found that the CMR keeps constant as a function of radius within the cluster. In particular, the CMR of Perseus has slope and zero-point consistent with those reported for Fornax (Mieske et al. 2007), Hydra I (Misgeld et al. 2008) and Centaurus (Misgeld et al. 2009). Such linearity and universality led several authors to use the CMR as a reliable distance indicator (Sandage 1972) and to suggest that the origin of this relation in galaxy clusters is independent of the environment (Paper I; Misgeld et al. 2008; De Rijcke et al. 2009).

However, for the Virgo cluster, Janz & Lisker (2009) have obtained an S-shaped CMR that seems to be consistent with the non-linear relation found by Ferrarese et al. (2006) for the same cluster. In addition, it is still under discussion whether there is a genuine (i.e. with a physical origin) increase in the scatter of the CMR towards its faint end or, instead, the larger scatter can be accounted for by photometric or classification errors and/or background galaxies contamination.

In the Perseus cluster, Conselice et al. (2002) have found a significant spread ($\sigma_{(B-R)} \sim 0.5$ mag) around the mean CMR, in the colours of galaxies with $M_B > -16$ mag. They argued in favour of a physical origin of this scatter, pointing to differences in metal abundances and formation scenarios among blue and red low-mass cluster galaxies. From a more recent spectroscopic study of the faint population of Perseus, Penny & Conselice (2008) have found that most of the red and blue galaxies responsible of the scatter are in the background. However, there is still an increase in the colour dispersion of confirmed members with $M_B > -15$ mag, in comparison with brighter ones. Janz & Lisker (2009) found an increase of the scatter about the CMR at intermediate brightness, while for the brighter and fainter galaxies the scatter is interpreted as due to photometric errors. The authors conclude that the increase at

intermediate luminosities confirms the fact that, in Virgo, dwarf and bright early-type galaxies do not share one common linear CMR.

In contrast, from a thorough morphological identification of the galaxies included in the Coma CMR, Terlevich et al. (2001) have found no detectable increase in the colour dispersion all along the early-type galaxies' relation. When spiral and irregular galaxies, as well as unclassified objects, are plotted in the same colour–magnitude diagram, they introduce a considerable scatter towards the blue side of the relation at intermediate and low luminosities. Andreon et al. (2006) have obtained a thin ($\sigma_{(B-R)} = 0.04$ mag) CMR in Abell 1185, with a scatter that does not increase with magnitude. López-Cruz et al. (2004) have found, for 57 X-ray-detected Abell clusters in the redshift range $0.02 \leq z \leq 0.18$, a universal CMR with an average colour dispersion of $\sigma_{(B-R)} = 0.074$ mag. They noticed that the cluster displaying the largest scatter in its CMR (0.5 mag at $R = 18$ mag) presents background contamination from higher redshift clusters. These authors also pointed out that photometric errors could become an important source of dispersion in the relation (see, also, Secker et al. 1997). In the Hydra (Misgeld et al. 2008) and Centaurus (Misgeld et al. 2009) clusters, a larger colour scatter has also been found for faint early-type galaxies, in comparison to luminous ones. However, such increase is considered as due to photometric errors and it is shown that dubious members of the cluster and background galaxies can introduce significant dispersion in the relation. Recently, Jaffé et al. (2011) have found that 172 early-type confirmed members of 13 clusters and groups with redshifts $0.4 \lesssim z \lesssim 0.8$ define tight CMRs with a small intrinsic colour scatter ($\sigma_{(U-V)} = 0.076$).

5.1.3 The CMR in Antlia

The CMR of spectroscopically confirmed Antlia members displays the most common features found for this relation in other nearby and distant clusters of galaxies. That is, it spans almost 10 mag with no perceptible change of slope or increase in its scatter towards faint luminosities. When unconfirmed members and confirmed background galaxies are introduced in the relation, it displays a larger colour dispersion, not only in its faint end but also at intermediate luminosities. In fig. 2b of Paper I we included in the same colour–magnitude diagram FS90 galaxies with spiral and irregular morphologies, some of them with spectroscopically confirmed membership. These objects introduced considerable dispersion towards the blue side of the relation, in agreement with the results of Terlevich et al. (2001).

The revised slope of the relation for all definite members is steeper than that found in Paper I. However, this value is in agreement with the one found in that paper for the bright end of the relation. Therefore, the bright galaxies seem to define the slope of the relation and when confirmed early-type dwarf members are included in the analysis, the faint galaxies follow a relation with a similar slope and scatter. This steeper value for the slope of the CMR of Antlia is still consistent with those reported for other galaxy clusters.

The computed intrinsic scatter of the relation is $\sigma_{(C-T_1)} \sim 0.08$ when only confirmed members are considered. Following Terlevich et al. (2001, see their equation 1), we calculate the intrinsic scatter as $\sigma_{\text{intr}} = \sqrt{\sigma_{\text{obs}}^2 - \langle \epsilon \rangle^2}$, where $\langle \epsilon \rangle$ is the mean colour error of the sample. If we translate our intrinsic dispersion to $(B - R)$ colours through $\sigma_{(B-R)} = 0.704\sigma_{(C-T_1)}$ (see equation 8 in Forte, Faifer & Geisler 2007), we obtain $\sigma_{(B-R)} \sim 0.06$, which is similar to the mean value obtained by López-Cruz et al. (2004) for clusters with $z < 0.04$, and consistent with the value obtained by Penny & Conselice (2008) for the CMR of Perseus at the bright end ($\sigma_{(B-R)} \sim 0.05$).

If we take into account that $T_1 - R \simeq 0.02$ (Geisler 1996), we can use the relation $\sigma_{(V-T_1)} = \sigma_{(V-R)} = 0.256\sigma_{(C-T_1)}$ (see equation 1 in Harris et al. 2002) and we obtain $\sigma_{(V-R)} \sim 0.02$, which is a lower value than that obtained by Andreon et al. (2006) in Abell 1185 ($\sigma_{(V-R)} = 0.036$). In the Centaurus cluster, Misgeld et al. (2009) have found intrinsic scatters of $\sigma_{(V-I)} = 0.06, 0.09$ and 0.14 in three different magnitude intervals. Using $\sigma_{(V-I)} = 0.49\sigma_{(C-T_1)}$ (see the first equation in Forbes & Forte 2001), these values translate in $\sigma_{(C-T_1)} = 0.12, 0.18$ and 0.28 , much higher than our common value for the whole Antlia CMR. For the Hydra cluster, Misgeld et al. (2008) have found a mean scatter for the relation of $\sigma_{(V-I)} = 0.12$, which is equivalent to $\sigma_{(C-T_1)} = 0.24$.

5.1.4 cE's location in the CMR

Regarding the positions in the colour–magnitude diagram of the confirmed Antlia cEs, they can be compared with those displayed by the cE galaxies recently identified in Centaurus (Misgeld et al. 2009) and Coma (Price et al. 2009, see also Chiboucas et al. 2010). Centaurus' cEs are located within the CMR on its red side, in a similar manner to Antlia's cEs (see fig. 3 in Misgeld et al. 2009). Despite all confident Coma's cEs (namely, CcGV9a, CcGV19a and CcGV19b) are found on the red side of Coma's mean CMR, only one of them shows a similar location to those found in Antlia and Centaurus (that is, within or near the general trend), while the other two display a considerable offset from the mean relation towards redder colours and/or fainter brightnesses (see fig. 2 in Price et al. 2009).

Coma's cEs have age and abundance estimations. All three galaxies are coeval within the age estimation errors. CcGV9a and CcGV19b present similar $(B - I)$ colours, and similar [Fe/H] and [Mg/Fe] abundances, while CcGV19a is the reddest cE galaxy in the association, with the highest [Fe/H] and [Mg/Fe] values. Therefore, the different locations of these three cEs in the colour–magnitude diagram can be explained through abundance differences and/or luminosity fading.

In this context it is interesting to point out that Faber (1973) noticed that *a small number of peculiar dwarf ellipticals are known that are quite red and have unusually high surface brightness* and that these objects *clearly do not fit into the sequence of normal ellipticals*. Moreover, Faber considered that these systems *are in fact remnants of tidal encounters with more massive companion galaxies*.

5.1.5 The scatter of the CMR

Given the universality of the CMR in clusters of galaxies, if the increase in the scatter at low luminosities has a physical origin, it should be observed at the same absolute magnitude in all cases. Secker et al. (1997) have obtained a CMR for the Coma cluster with a scatter that increases faintwards from $R \simeq 19.5$ mag, corresponding to $M_R = -15.5$ mag with a distance modulus $(m - M) = 35$. In the Perseus cluster, the scatter increases significantly at $M_B = -15$ mag (see fig. 3 in Penny & Conselice 2008). By means of the transformations given by Fukugita et al. (1995), this is equivalent to $M_R = -16.6$ mag. In Fornax, Hilker et al. (2003) and Mieske et al. (2007) have found an increase of the CMR scatter at $M_V \simeq -12.5$ mag or $M_R \simeq -13.1$ mag. In Hydra, the increase in the scatter is significant from $M_V \simeq -14$ mag (fig. 10 in Misgeld et al. 2008) or $M_R \simeq -14.6$ mag. In Centaurus, it is from $M_V \simeq -13$ mag or $M_R \simeq -13.6$ mag (fig. 3 in Misgeld et al. 2009). In Virgo, the

peak of the dispersion is found at $M_r = -17$ mag which is equivalent to $M_R \sim -17.3$ mag. In our case, the faintest Antlia confirmed members and candidates introduce a detectable dispersion increase starting from $M_R \sim -15$ mag.

Therefore, in all these clusters, the increase of the scatter starts at different absolute magnitudes, which tend to be brighter for more distant clusters, if Virgo is excluded from the sample. This trend could be interpreted as a diminishing of the precision of the photometric data and a more uncertain morphological/membership classification as we go to more distant clusters.

From the analysis performed in Section 5.1.3, it might be inferred that, once photometric errors are discounted, different CMRs obtained using metallicity sensitive colours, such as $(C - T_1)$ and $(B - R)$, display fairly low intrinsic dispersions ($\sigma_{(C-T_1)} < 0.08$ mag).

Several processes have been proposed as responsible for the intrinsic scatter of the relation (e.g. differences in ages, Terlevich et al. 1999, Ferreras & Silk 2003, Romeo et al. 2008; minor mergers, Kaviraj et al. 2009; accretion of small amounts of gas at high redshifts, Pipino & Matteucci 2006). Whatever the process dominating the intrinsic scatter is, from our comparison we could state that it arises with similar strength in different clusters. In this sense, Jaffé et al. (2011) have found a colour scatter with no evolution with redshift or correlation with the velocity dispersions of the clusters included in their analysis.

5.2 Luminosity- $\langle\mu_{\text{eff}}\rangle$ relation

5.2.1 Antlia's relation

As shown in Section 4.2, in a plot of T_1 magnitude versus $\langle\mu_{\text{eff}}\rangle$, FS90 early-type dwarf members of Antlia follow the locus of constant effective radius of 1 kpc down to $T_1 \sim 18$ mag. Fainter FS90 members tend to deviate from this locus towards smaller radii. All of the new dwarf galaxy members, which have luminosities fainter than $T_1 = 18$ mag, show the same behaviour. The mean effective radius of the confirmed members with $T_1 > 18$ mag is $\langle r_{\text{eff}} \rangle = 0.58$ (rms 0.26) kpc. Therefore, there seems to be a faint limit in magnitude for the constant effective radius relation followed by dEs.

We have already mentioned that this could be due to the isophotal limit of our photometry. It is possible that we are not reaching the most external regions of the galaxies as they are embedded in the background. Many of these faint objects are located near brighter galaxies as well. In this way, our effective radius could be underestimated for galaxies fainter than $T_1 \sim 18$ mag ($M_V \sim -14.1$ mag; Fukugita et al. 1995), leading to the apparent discontinuity or ‘break’ in this relation.

However, Chiboucas, Karachentsev & Tully (2009) have found that newly discovered dwarf galaxies in the M81 Group ($D = 3.6$ Mpc) have effective radii in agreement to those found for the new dwarf galaxies in Antlia, i.e. $r_{\text{eff}} \lesssim 0.5$ kpc (see their table 3). Local Group dSphs have $r_{\text{eff}} \lesssim 0.5$ kpc as well (Zaritsky, González & Zabludoff 2006 and references therein). Cellone & Buzzoni (2005) as well as De Rijcke et al. (2009) found a similar trend to our faint break, in their respective samples of dwarf galaxies. Therefore, we cannot rule out the possibility that the luminosity versus $\langle\mu_{\text{eff}}\rangle$ relation, corresponding to a mean constant effective radius of ~ 1 kpc, presents two physical breaks: one at magnitudes brighter than $M_R \sim -20$ mag, and another at its faint end, at magnitudes fainter than $M_R \sim -14$ mag. We recall that the correlation between luminosity and $\langle\mu_{\text{eff}}\rangle$ for magnitudes brighter

than $M_R \sim -20$ mag corresponds to the Kormendy (1977b) scaling relation defined by bright Es and bulges of S galaxies on the r_{eff} versus μ_{eff} diagram. This is a projection of the Fundamental Plane of E galaxies.

As mentioned above in this section, most of the galaxies fainter than the low-luminosity break are located near brighter ones. The smaller r_{eff} found in our faint candidates might then be related with tidal effects. The newly confirmed cE galaxies also deviate from the locus followed by the rest of early-type dwarfs of similar luminosities towards smaller effective radii. They are companions of the giant ellipticals that dominate the central region of the cluster. In Paper II we showed that one of them, FS90 110, displays a low-surface-brightness bridge that links it with NGC 3258, confirming the existence of an interaction between both galaxies. Surface brightness profiles displaying a break, as is the case of FS90 110 (see Paper II), would favour this interpretation (Choi, Guhathakurta & Johnston 2002; Mieske et al. 2006).

5.2.2 Dichotomy between E and dE galaxies

Graham & Guzmán (2003) have argued that, with the exception of the very bright galaxies ($M_B \lesssim -20.5$, $M_V \lesssim -21.5$, i.e. ‘core’ E), the break at the bright end of the luminosity versus $\langle\mu_{\text{eff}}\rangle$ relation is not due to different formation mechanisms among dwarf and bright E galaxies. They emphasize that both types of galaxies display continuous trends in the central surface brightness (μ_0) versus luminosity plot, and in the n Sérsic index (Sérsic 1968) versus luminosity diagram. This would show that dEs are the low-luminosity extension of E galaxies. Graham & Guzmán (2003) explain the different behaviour of Es and dEs in the luminosity- $\langle\mu_{\text{eff}}\rangle$ space as due to an increasing difference between μ_0 and $\langle\mu_{\text{eff}}\rangle$ values with increasing n as we go from dE to E (without core) systems (see their figs 11 and 12).

In contrast, Kormendy et al. (2009) sustain the existence of a dichotomy between dE (*spheroidal* galaxies in their paper) and E galaxies pointing to distinct origins. The fact that E and dE follow similar correlations would indicate that the parameters involved in such relations are not sensitive to the physics that makes them different. Therefore, these authors consider that to distinguish galaxy types, it is necessary to use all parameter correlations and find out which ones are sensitive to formation mechanisms. From an extensive analysis, Kormendy et al. (2009) conclude that E galaxies form via mergers being cE galaxies their low-luminosity counterparts, while dEs are late-type galaxies transformed by environmental effects and energy feedback from supernovae.

In this context, it is interesting to point out the top panel of fig. 1 in the work by Chilingarian et al. (2009). There, the authors show the location in the $\langle\mu_{\text{eff}}\rangle$ -luminosity diagram of all cEs detected by them with the Virtual Observatory (21 objects), along other confirmed cEs and early-type systems. It can be seen that M32 seems to extend the locus defined by bright early-type galaxies towards brighter values of $\langle\mu_{\text{eff}}\rangle$ (or smaller r_{eff}). But the rest of the cEs included in the plot seem to define a parallel sequence to that of dEs and dS0s, towards brighter $\langle\mu_{\text{eff}}\rangle$. Simulating the interaction of a disc galaxy with a galaxy cluster potential, Chilingarian et al. (2009) also found that tidal stripping can reduce the stellar mass of the galaxy and speculate that low-luminosity objects could be the progenitors of cEs. Considering that most (if not all) cEs are companions of brighter galaxies, it might be interpreted that the offset of different cE galaxies from the dE/dS0 sequence depends on the degree of interaction experienced by the system and/or on the

morphology of the progenitor. In this sense, cE galaxies would not be thought as the natural extension of the family of giant ellipticals towards low luminosities, as the origins of both populations would be quite different. It is worth noting that our two cE galaxies also seem to lie along a sequence parallel to that of dEs rather than to follow the trend of bright ellipticals.

It is clear that the interpretation of the behaviour of bright and dwarf early-type galaxies in the luminosity–(μ_{eff}) diagram is an open question. Our present results for the Antlia cluster do not show any discontinuity between bright and dwarf ones in this diagram, but it should be taken into account that bright early-type galaxies in Antlia are mainly lenticulars, not ellipticals. In addition, we should enlarge the photometric sample at the low-luminosity end before arriving at sensible conclusions.

At the moment, it is not possible to discern if $\langle \mu_{\text{eff}} \rangle$ keeps almost constant from the faint break towards fainter magnitudes, or if the effective surface brightness increases with decreasing luminosity, showing a similar trend to that displayed by E galaxies. However, it is remarkable the good match showed by the galaxies belonging to poor groups to the locus of constant effective radius defined by Antlia’s systems. This fact points to a relation that arises with similar characteristics in very different environments.

5.3 Projected galaxy distribution

X-ray observations of the Antlia cluster (Pedersen, Yoshii & Sommer-Larsen 1997; Nakazawa et al. 2000) have shown that the X-ray diffuse emission is elongated in the direction defined by a line joining both dominant galaxies. Studies of the globular cluster systems of NGC 3258 and NGC 3268 (Dirsch et al. 2003; Bassino et al. 2008) have revealed that these systems display an elongated distribution in the same direction. These results may be the consequence of tidal forces between both galaxies, which may be ultimately pointing to an ongoing merger in the central region of Antlia. Thus, the two structures found in this region (Fig. 4) might be two groups in interaction: one with NGC 3258 as dominant galaxy and another with NGC 3268 as the central galaxy, both of them containing a cE galaxy. More radial velocities from galaxies in the outer regions of Antlia are needed to confirm this hypothesis.

We have shown in Section 4.3 that there is no conclusive evidence of the existence of a colour–density relation in Antlia in the sense reported by Barazza et al. (2009) for Abell 901/902. These authors propose that the existence of this relation in the projected radial distribution is an indication that the formation of dEs is closely related to the processes that affect the cluster itself, such as ram-pressure stripping and harassment. The ram-pressure stripping would remove more efficiently (and faster) the interstellar medium of galaxies located closer to cluster centres. That may affect star formation in a way that these galaxies would have, on the average, an older stellar population and thus be redder than galaxies located further away from the cluster centres.

The harassment scenario predicts a colour gradient in terms of effective radius (Mastropietro et al. 2005), in the sense that bluer (outskirts) galaxies display larger r_{eff} than the redder (central) ones. In agreement with Barazza et al. (2009) results, we do not find a relation between colour and effective radius. In this context, as the early-type dwarf galaxy populations of Antlia and Abell 901/902 do not show such a gradient, the harassment process seems not to be a dominant one in these associations. Bosselli et al. (2008) have also found that the lack of correlations with cluster-centric distances in

the scaling relations favours a ram-pressure stripping scenario for the evolution of the galaxies.

5.4 dSph candidates in Antlia

Our selection of the low-luminosity dSph candidates in Antlia was mainly based on their limiting magnitude ($M_V \gtrsim -13$ mag; Kalirai et al. 2010) and morphology (diffuse appearance and no nucleus). Local Group counterparts of these objects are also devoid of gas and dominated by old and intermediate-age stars. Their extended sizes, low luminosity and measured velocity dispersions, as well as their large mass-to-light ratios, point to dSph being objects with large amounts of dark matter (e.g. Mateo 1998).

Our new dSph candidates have integrated magnitudes in the range of $T_1 = 20.2\text{--}22.3$ mag, which corresponds to $-10.4 \gtrsim M_R \gtrsim -12.5$. In agreement with the tidal origin proposed for dSph galaxies (e.g. Peñarrubia et al. 2009), they appear to cluster tightly around massive galaxies. In the Local Group, most dSphs are located within a radius of 300 kpc from the Milky Way and M31 (Gallagher & Wyse 1994; Grebel 2005). Though our dSph candidates sample in Antlia is in fact small, their positions displayed in Fig. 4 and identified by open pentagons place them close to the two giant dominant galaxies or to bright lenticulars, all of them confirmed cluster members. Their average projected distance to the closest bright galaxy (with $T_1 < 13$ mag) is 6.4 ± 1.3 arcmin, which at the Antlia distance corresponds to about ≈ 65 kpc.

Regarding their sizes, the study of dSphs in M31 by McConnachie & Irwin (2006b) has shown that their tidal radii ($\approx 1.2\text{--}7$ kpc) are about twice as extended as their counterparts in the Milky Way. The classical dSphs (i.e. not including the newly discovered ultra-faint dwarfs) surrounding the Milky Way have tidal radii in the range of ~ 0.5 to 3 kpc (Irwin & Hatzidimitriou 1995). Even their spatial distribution is different, the Milky Way satellites being more clustered around their host than those of M31 (McConnachie & Irwin 2006a).

Globally, we can consider that tidal radii of Local Group dSphs range from ~ 0.5 to 7 kpc, which correspond to $\approx 3\text{--}45$ arcsec at the Antlia distance. From Table B2, we can see that the Antlia dSph candidates display total radii in the range of 5–11 arcsec, which is within the expected values if we compare to the Local Group ones, though in the range of the smaller sizes. This can be understood like a selection effect, as it would be even more difficult to detect larger, but more diffuse, galaxies at the Antlia distance.

6 SUMMARY AND CONCLUSIONS

In this paper we have deepened our study of the galaxy populations in the central region of the Antlia cluster, paying particular attention to the faint systems composed by dwarf ellipticals and dwarf spheroidals. We have obtained radial velocities for a total of 28 faint galaxies ($M_V \gtrsim -18$ mag) located in this region through Gemini-GMOS and Magellan-MIKE spectra. With these pieces of new information, we have improved the colour–magnitude and surface brightness versus luminosity relations originally studied in Paper I, and we have analysed the projected spatial distribution of the whole galaxy sample, presenting Washington photometry for five newly confirmed members from the FS90 catalogue as well as for 16 new low-surface-brightness candidates that have never been catalogued before. Total and/or effective radii have been measured for the five new members and the 16 new candidates except one. In addition,

images in the R band are shown for all the galaxies with new radial velocities and the 16 new candidates. Our main conclusions are as follows.

(i) Early-type galaxies in the Antlia cluster follow a tight colour–magnitude relation that extends, with no perceptible change of slope, from the giant ellipticals down to the dSphs spanning almost 12 mag in luminosity. When only confirmed early-type members are considered, we find no significant increase in the scatter towards the faint end of the relation. When the intrinsic scatter of the CMR of Antlia is compared with those of other groups and clusters’ CMRs, it is found that Antlia’s CMR is one of the tightest relations reported up to now. We suggest that this finding is related with the use of a metallicity-sensitive colour index such as $(C - T_1)$.

(ii) The five previously unknown early-type Antlia members and the 16 new candidates follow the same photometric relations as the FS90 early-type members and candidates, although introducing some dispersion. In particular, the new dwarf candidates increase the scatter of the CMR towards its faint end. These new dwarf members and candidates also depart, towards smaller effective radii, from the surface brightness versus luminosity relation traced by FS90 dE galaxies with $14 < T_1 < 18$ that follow the locus of constant effective radius of ≈ 1 kpc. The latter effect could be due to the isophotal limit of our photometry. However, similar sizes ($r_{\text{eff}} < 1$ kpc) have been reported for faint members of the Local Group, M81 and NGC 5044 groups. Therefore, there seems to exist a physical brightness limit for the relation corresponding to constant effective radius, a relation that seems to arise in different environments as it has been found in clusters such as Virgo and Coma (see fig. 5 in Paper I) as well as in poor groups.

(iii) With regard to the possible existence of a discontinuity between bright and faint ellipticals in the surface brightness versus luminosity relation (e.g. Graham & Guzmán 2003; Kormendy et al. 2009), our results for the Antlia cluster do not show any gap in this diagram. It should be taken into account that the bright early-type galaxies in Antlia are mostly lenticular galaxies and few ellipticals.

(iv) The dE galaxies with $13 < T_{10} < 18$ present an almost constant effective radius around $\langle r_{\text{eff}} \rangle \approx 0.9$ kpc, irrespective of whether their colours are bluer or redder than that of the mean CMR for the same luminosity. The almost constant effective radii of dEs are in agreement with what has been found for other clusters and groups (Paper I and references therein). For galaxies fainter than $T_{10} = 18$ mag, the mean value decreases to $\langle r_{\text{eff}} \rangle \approx 0.6$ kpc, which is consistent with what is found for the faintest galaxies in the Local Group, M81 and NGC 5044 groups.

(v) We have not found a colour–density or a colour–size relation among our Antlia dwarf galaxy sample. This behaviour might favour a ram-pressure stripping scenario for the evolution of dwarf galaxies in this cluster. However, we should confirm these trends by enlarging our dwarf galaxy sample considering dwarf galaxies present in the outer regions of the cluster.

(vi) We have confirmed the existence of two cE galaxies in Antlia. Each of them is the neighbour of one of the two giant ellipticals that dominate the central region of Antlia. For their luminosities, they are both the reddest and most compact objects of the early-type Antlia galaxies. If we accept that their colours are mainly driven by metallicity, as likely happens with galaxies on the CMR, both of them would be the richest galaxies for their luminosities in our sample. The cEs found in the Centaurus and Coma clusters are also located on the red side of their corresponding mean CMRs.

However, the cE galaxies found in Coma present [Fe/H] abundances comparable to those of some dEs. Therefore, at the moment it is difficult to establish if cEs should be treated as a separate class of objects, or should be considered as part of the general early-type dwarf galaxy family experiencing, perhaps, particular dynamical processes.

(vii) We have found a small sample of seven unstudied dSph candidates, whose membership cannot be confirmed with our spectra due to their low surface brightness. They cover a range in integrated magnitudes $-10.4 \gtrsim M_R \gtrsim -12.5$ and total radii between 5 and 11 arcsec, which at the Antlia distance correspond to approximately 850 pc–2 kpc. They are found close to bright galaxies ($T_1 < 13$ mag), their average projected distance from them being ≈ 65 kpc.

(viii) The projected spatial distribution of the whole sample points to a complex structure for Antlia. At least two groups are present in the central region, with some evidence of an ongoing merger. We will extend our study adding new fields adjoining the central one, and increasing the spectroscopic data set, in order to add kinematic information to the spatial distribution.

ACKNOWLEDGMENTS

We are grateful to the anonymous referee for his/her comments and corrections that helped to improve the content of this paper. AVSC and GAR warmly thank Nidia Morrell for her help with the reduction of echelle spectra. AVSC and FRF acknowledge financial support from Agencia de Promoción Científica y Tecnológica of Argentina (BID AR PICT 2010-0410 and BID AR PICT 2007-885). TR acknowledges financial support from the Chilean Center for Astrophysics, FONDAF no. 15010003, from FONDECYT project no. 1100620 and from the BASAL Centro de Astrofísica y Tecnologías Afines (CATA) PFB-06/2007. GAR was supported by ALMA/Conicyt (grant 31070021) and ESO/Comite Mixto. This work was also funded with grants from Consejo Nacional de Investigaciones Científicas y Técnicas de la República Argentina, Agencia Nacional de Promoción Científica y Tecnológica and Universidad Nacional de La Plata (Argentina). The Gemini data used in this paper were obtained under Gemini programs GS-2008A-Q-56, GS-2009A-Q-25 and GS-2010A-Q-21.

REFERENCES

- Andreon S., Cuillandre J.-C., Puddu E., Mellier Y., 2006, *MNRAS*, 372, 60
 Annibali F., Grützbauch R., Rampazzo R., Bressan A., Zeilinger W. W., 2011, *A&A*, 528, A19
 Barazza F. D. et al., 2009, *A&A*, 508, 665
 Bassino L. P., Richtler T., Dirsch B., 2008, *MNRAS*, 386, 1145
 Baum W., 1959, *PASP*, 71, 106
 Belokurov V. et al., 2008, *ApJ*, 686, L83
 Bertin E., Arnouts S., 1996, *A&AS*, 117, 393
 Binggeli B., Jerjen H., 1998, *A&A*, 333, 17
 Binggeli B., Sandage A., Tammann G. A., 1985, *AJ*, 90, 1681
 Boselli A., Boissier S., Cortese L., Gavazzi G., 2008, *A&A*, 489, 1015
 Bower R. G., Lucey J. R., Ellis R. S., 1992, *MNRAS*, 254, 601
 Buzzoni A., Cellone S., Saracco P., Zucca E., 2011, *MNRAS*, submitted
 Caldwell N., Bothun G. D., 1987, *AJ*, 94, 1126
 Cellone S. A., 1999, *A&A*, 345, 403
 Cellone S. A., Buzzoni A., 2001, *A&A*, 369, 742
 Cellone S. A., Buzzoni A., 2005, *MNRAS*, 356, 41
 Chiboucas K., Mateo M., 2006, *AJ*, 132, 347
 Chiboucas K., Karachentsev I. D., Tully R. B., 2009, *AJ*, 137, 3009
 Chiboucas K., Tully R. B., Marzke R. O., Trentham N., Ferguson H. C., Hammer D., Carter D., Khosroshahi H., 2010, *ApJ*, 723, 251

- Chilingarian I. V., Bergond G., 2010, MNRAS, 405, L11
- Chilingarian I., Cayatte V., Revaz Y., Dodonov S., Durand D., Durret F., Micol A., Slezak E., 2009, Sci, 326, 1379
- Choi P. I., Guhathakurta P., Johnston K. V., 2002, AJ, 124, 310
- Clemens M., Panuzzo P., Rampazzo R., Vega O., Bressan A., 2011, MNRAS, 412, 2063
- Conselice C. J., Gallagher J. S., Wyse R. F. G., 2002, AJ, 123, 2246
- Conselice C. J., Gallagher J. S., Wyse R. F. G., 2003, AJ, 125, 66
- De Rijcke S., Penny S. J., Conselice C. J., Valcke S., Held E. V., 2009, MNRAS, 393, 798
- Dirsch B., Richtler T., Bassino L. P., 2003, A&A, 408, 929
- Faber S. M., 1973, ApJ, 179, 731
- Ferguson H. C., 1989, Ap&SS, 157, 227
- Ferguson H. C., Binggeli B., 1994, A&AR, 6, 67
- Ferguson H. C., Sandage A., 1990, AJ, 100, 1 (FS90)
- Ferrarese L. et al., 2006, ApJS, 164, 334
- Ferreras I., Silk J., 2003, MNRAS, 344, 455
- Forbes D., 2007, in Saviane I., Ivanov V. D., Borissova J., eds, Groups of Galaxies in the Nearby Universe (ESO Astrophysics Symposia). Springer-Verlag, Berlin, p. 97
- Forbes D., Forte J. C., 2001, MNRAS, 322, 257
- Forte J. C., Faifer F. R., Geisler D., 2007, MNRAS, 382, 1947
- Fukugita M., Shimasaku K., Ichikawa T., 1995, PASP, 107, 945
- Gallagher J. S., Wyse R. F. G., 1994, PASP, 106, 1225
- Geisler D., 1996, AJ, 111, 480
- Graham A. W., 2002, ApJ, 568, L13
- Graham A. W., 2011, EAS Publ. Ser., 48, 231
- Graham A. W., Guzmán R., 2003, AJ, 125, 2936
- Grebel E. K., 2005, in Jerjen H., Binggeli B., eds, Proc. IAU Colloq. 198, Near-Field Cosmology with Dwarf Elliptical Galaxies. Cambridge Univ. Press, Cambridge, p. 1
- Harris W. E., Harris G. L. H., Holland S. T., McLaughlin D. E., 2002, AJ, 124, 1435
- Hilker M., Mieske S., Infante L., 2003, A&A, 397, L9
- Howell J., 2005, AJ, 130, 2065
- Huxor A. P., Phillipps S., Price J., Harniman R., 2011, MNRAS, 414, 3557
- Irwin M., Hatzidimitriou D., 1995, MNRAS, 277, 1354
- Jaffé Y. L., Aragón-Salamanca A., De Lucia G., Jablonka P., Rudnick G., Saglia R., Zaritsky D., 2011, MNRAS, 410, 280
- Janz J., Lisker T., 2009, ApJ, 696, L102
- Kalirai J. S. et al., 2010, ApJ, 711, 671
- Kaviraj S., Peirani S., Khochfar S., Silk J., Kay S., 2009, MNRAS, 394, 1713
- Kormendy J., 1977a, ApJ, 217, 406
- Kormendy J., 1977b, ApJ, 218, 333
- Kormendy J., Fisher D. B., Cornell M. E., Bender R., 2009, ApJS, 182, 216
- Lisker T., Glatt K., Westera P., Grebel E., 2006, AJ, 132, 2432
- Lisker T., Grebel E. K., Binggeli B., 2008, AJ, 135, 380
- López-Cruz O., Barkhouse W. A., Yee H. K. C., 2004, ApJ, 614, 679
- Mastropietro C., Moore B., Mayer L., Debattista V. P., Piffaretti R., Stadel J., 2005, MNRAS, 364, 607
- Mateo M. L., 1998, ARA&A, 36, 435
- McConnachie A. W., Irwin M. J., 2006a, MNRAS, 365, 902
- McConnachie A. W., Irwin M. J., 2006b, MNRAS, 365, 1263
- Mendel J. T., Proctor R. N., Forbes D. A., Brough S., 2008, MNRAS, 389, 749
- Mendel J. T., Proctor R. N., Rasmussen J., Brough S., Forbes D., 2009, MNRAS, 396, 2103
- Mieske S. et al., 2006, ApJ, 653, 193
- Mieske S., Hilker M., Infante L., Mendes de Oliveira C., 2007, A&A, 463, 503
- Misgeld I., Mieske S., Hilker M., 2008, A&A, 486, 697
- Misgeld I., Hilker M., Mieske S., 2009, A&A, 496, 683
- Nakazawa K., Makishima K., Fukazawa Y., Tamura T., 2000, PASJ, 52, 623
- Pedersen K., Yoshii Y., Sommer-Larsen J., 1997, ApJ, 485, L17
- Peñarrubia J., Navarro J. F., McConnachie A. W., 2008, ApJ, 673, 226
- Peñarrubia J., Navarro J. F., McConnachie A. W., Martin N., 2009, ApJ, 698, 222
- Penny S. J., Conselice C., 2008, MNRAS, 383, 247
- Penny S. J., Conselice C., De Rijcke S., Held E., Gallagher J. S., III, O'Connell R. W., 2011, MNRAS, 410, 1076
- Pipino A., Matteucci F., 2006, MNRAS, 365, 1114
- Price J. et al., 2009, MNRAS, 397, 1816
- Romeo A. D., Napolitano N. R., Covone G., Sommer-Larsen J., Antonuccio-Delego V., Capaccioli M., 2008, MNRAS, 389, 13
- Sánchez-Blázquez P. et al., 2006, MNRAS, 371, 703
- Sandage A., 1972, ApJ, 176, 21
- Sandage A., Visvanathan N., 1978, ApJ, 223, 707
- Secker J., Harris W. E., Plummer J. D., 1997, PASP, 109, 1377
- Sérsic J. L., 1968, Atlas de Galaxias Australes. Observatorio Astronómico, Córdoba
- Smith Castelli A. V., Bassino L. P., Richtler T., Cellone S. A., Aruta C., Infante L., 2008a, MNRAS, 386, 2311 (Paper I)
- Smith Castelli A. V., Faifer F., Richtler T., Bassino L. P., 2008b, MNRAS, 391, 685 (Paper II)
- Smith Castelli A. V., Faifer F. R., Bassino L. P., Romero G. A., Cellone S. A., Richtler T., 2009, Bol. Asoc. Argent. Astron., 52, 229
- Terlevich A. I., Kuntschner H., Bower R. G., Caldwell N., Sharples R. M., 1999, MNRAS, 310, 445
- Terlevich A. I., Caldwell N., Bower R. G., 2001, MNRAS, 326, 1547
- Tolstoy E., Hill V., Tosi M., 2009, ARA&A, 47, 371
- Trager S., Faber S., Worthey G., Jesús González J., 2000, AJ, 120, 165
- Trujillo I., Graham A. W., Caon N., 2001, MNRAS, 326, 869
- Visvanathan N., Sandage A., 1977, ApJ, 216, 214
- Zaritsky D., Gonzalez A. H., Zabludoff A. I., 2006, ApJ, 642, L37

APPENDIX A: FS90 GALAXIES WITH NEW RADIAL VELOCITIES

In this appendix we present the new measured radial velocities of 23 FS90 galaxies (Table A1), as well as their logarithmic scale R images (Fig. A1).

Table A1. FS90 galaxies with new radial velocities.

	FS90 ID	α (J2000)	δ (J2000)	FS90 mor.	FS90 status	v_r (km s $^{-1}$)
1	FS90 70	10:28:06.9	−35:35:20	dE	1	2864 ± 70
2	FS90 83	10:28:23.0	−35:30:57	S or Sm	3	19685 ± 33
3	FS90 85	10:28:24.0	−35:34:22	dE	1	2000 ± 200
4	FS90 103	10:28:45.1	−35:34:40	dE	3	2054 ± 29
5	FS90 109	10:28:53.0	−35:32:52	dE	2	1618 ± 24
6	FS90 110	10:28:53.0	−35:35:34	E(M32?)	3	2911 ± 7
7	FS90 120	10:29:02.1	−35:34:04	ImV	1	2634 ± 13
8	FS90 123	10:29:03.1	−35:40:30	dE, N	2	1865 ± 25
9	FS90 133	10:29:12.0	−35:39:28	dE, N	1	2205 ± 24
10	FS90 136	10:29:15.3	−35:25:58	dE, N	1	2989 ± 10
11	FS90 137	10:29:15.1	−35:41:34	ImV	2	3987 ± 36
12	FS90 149	10:29:27.3	−35:27:10	S0 or dS0	3	46175 ± 13
13	FS90 188	10:30:02.4	−35:24:28	dE	1	2673 ± 17
14	FS90 192	10:30:04.5	−35:20:31	E(M32?)	3	2526 ± 4
15	FS90 196	10:30:06.4	−35:23:31	dE	1	3593 ± 9
16	FS90 205	10:30:18.4	−35:24:43	dE	2	45909 ± 18
17	FS90 209	10:30:19.4	−35:34:48	dE	2	3065 ± 13
18	FS90 212	10:30:21.3	−35:35:31	SmIII	1	2364 ± 27
19	FS90 213	10:30:21.6	−35:12:14	dE	2	2185 ± 21
20	FS90 221	10:30:25.4	−35:23:38	dE	2	3556 ± 130
21	FS90 223	10:30:25.6	−35:13:19	dE	1	2661 ± 9
22	FS90 227	10:30:31.4	−35:23:06	dE?	2	2921 ± 60
23	FS90 228	10:30:31.6	−35:14:38	dE, N	1	2417 ± 13

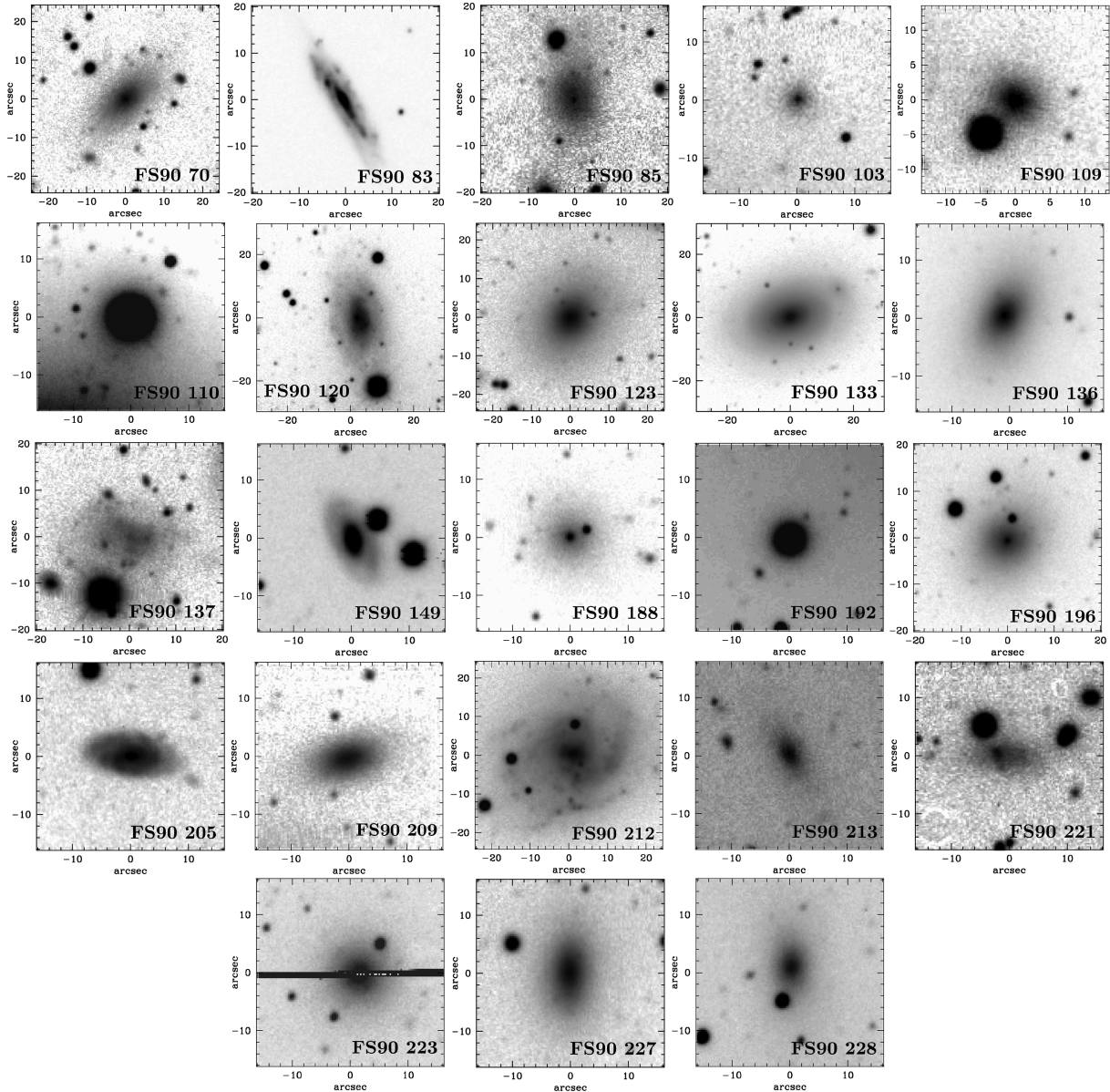


Figure A1. Logarithmic scale R images of FS90 galaxies with new radial velocities. North is up and east is to the left. Background galaxies are FS9083, FS90 149 and FS90 205. The rest are all Antlia members.

APPENDIX B: NEW DWARF GALAXY MEMBERS AND CANDIDATES

We present the coordinates, radial velocities and photometric parameters for five new dwarf galaxy members identified from spectroscopic data obtained with Gemini-GMOS (see Table B1). In Fig. B1 we show their logarithmic scale R images. All of them display a bright central region that could be associated with a nucleus.

We also show the photometric parameters (when available) for 16 new dwarf galaxy candidates (see Table B2) and their images in Fig. B2.

APPENDIX C: ELLIPSE VERSUS SEXTRACTOR

In Paper I, we have obtained the CMR from colours and magnitudes measured with SEXTRACTOR and ELLIPSE. Therefore, it is interesting

to quantify if there are significant differences between these two ways of obtaining photometry. To this aim, in Fig. C1 we show plots comparing T_1 magnitudes, $(C - T_1)$ colours and effective radii obtained with SEXTRACTOR and ELLIPSE.

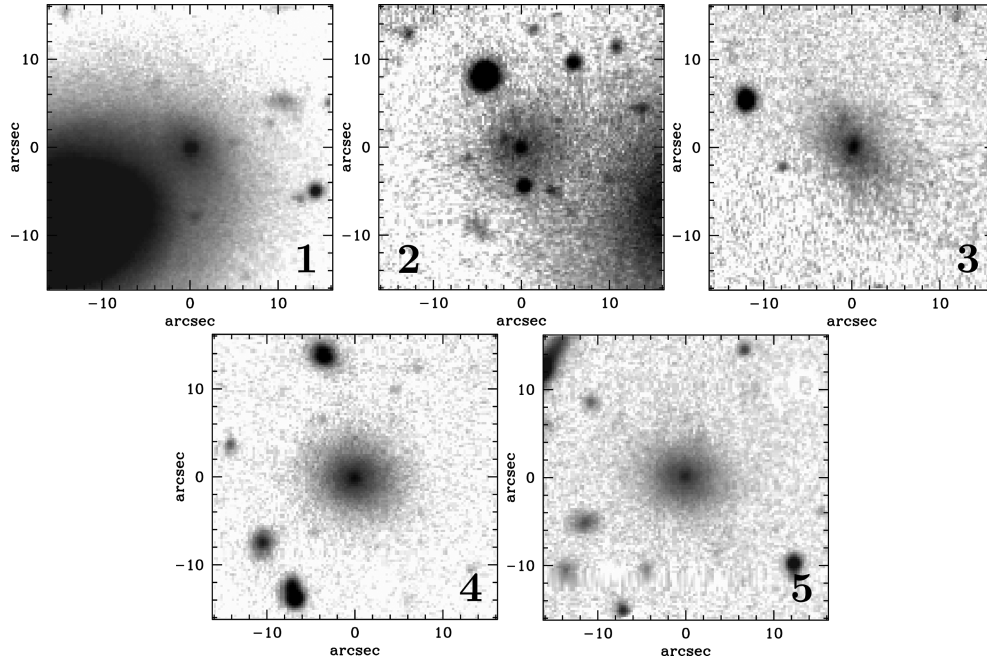
In the left panel of Fig. C1, we see that for luminosities in the range $12 \lesssim T_1 \lesssim 18$, magnitudes obtained from SEXTRACTOR and ELLIPSE agree well, the mean offset being $|\Delta T_1| = 0.08$. However, there are significant differences for $T_1 > 18$ mag, which can be as large as 1.14 mag. The mean offset for faint galaxies is $|\Delta T_1| = 0.44$ mag. In the case of C magnitudes (no plot is shown), considerable offsets arise for $C > 19$ mag. For magnitudes brighter than this limit, we obtained $|\Delta C| = 0.11$ and for fainter ones, $|\Delta C| = 0.45$ mag.

In the central panel of Fig. C1, we show the differences in $(C - T_1)$ colours as $\Delta(C - T_1) = (C - T_1)_{\text{SEX}} - (C - T_1)_{\text{ELL}}$ as a function of the ELLIPSE luminosity of the galaxy. For $T_1 > 16$ mag,

Table B1. New dwarf galaxy members located in the central region of the Antlia cluster.

ID	α (J2000)	δ (J2000)	$E(B - V)$	T_1 (mag)	$(C - T_1)$ (mag)	μ_{T_1} (mag arcsec $^{-2}$)	r_{T_1} (arcsec)	$\langle\mu_{\text{eff}}\rangle$ (mag arcsec $^{-2}$)	r_{eff} (arcsec)	v_r (km s $^{-1}$)	Remarks	
1	ANTL J102910–353920.1	10:29:10.3	−35:39:20.1	0.083	19.76 (0.02)	1.54 (0.03)	26.4	4.8	23.4	2.1	1940 ± 155	ELL
2	ANTL J102914–353923.6	10:29:14.4	−35:39:23.6	0.083	20.25 (0.06)	1.67 (0.08)	26.3	5.6	24.6	3.0	4067 ± 115	ELL
3	ANTL J103013–352458.3	10:30:13.8	−35:24:58.3	0.104	19.49 (0.04)	1.59 (0.06)	25.8	7.6	25.7	3.7	2613 ± 200	SE, NS
4	ANTL J103033–352638.6	10:30:33.3	−35:26:38.6	0.104	19.07 (0.02)	1.68 (0.04)	26.6	6.6	23.4	2.9	2311 ± 130	ELL
5	ANTL J103037–352708.8	10:30:37.5	−35:27:08.8	0.103	19.16 (0.03)	1.60 (0.04)	25.8	6.8	25.7	3.1	2400 ± 100	SE

Notes. Here, μ_{T_1} corresponds to the threshold above which SExtractor detects and measures the object (MU_THRESHOLD) or to the surface brightness of the outermost isophote for ELLIPSE. r_{T_1} is the radius that contains 90 per cent of the light for SExtractor or the equivalent radius ($r = \sqrt{ab} = a\sqrt{1-\epsilon}$) of the most external isophote for ELLIPSE. In both cases, $\langle\mu_{\text{eff}}\rangle$ is obtained from r_{eff} , the radius that contains one-half of the light (see equation 1 in Paper I) and is the output parameter FLUX_RADIUS for SExtractor. Remarks refer to SE = magnitudes and colours measured with SExtractor; ELL = magnitudes and colours obtained from ELLIPSE and NS = nearby a bright star.

**Figure B1.** Logarithmic scale R images of newly confirmed dwarf members of Antlia. They are identified by a number at one of the lower corners, which corresponds to the order number in Table B1. North is up and east is to the left.**Table B2.** New dwarf galaxy candidates with early-type morphologies located in the central region of the Antlia cluster.

ID	α (J2000)	δ (J2000)	$E(B - V)$	T_1 (mag)	$(C - T_1)$ (mag)	μ_{T_1} (mag arcsec $^{-2}$)	r_{T_1} (arcsec)	$\langle\mu_{\text{eff}}\rangle$ (mag arcsec $^{-2}$)	r_{eff} (arcsec)	Remarks	
1	ANTL J102828–354128	10:28:28.2	−35:41:28.5	0.074	18.15 (0.05)	1.63 (0.07)	25.7	14.8	24.4	7.3	SE
2	ANTL J102839–351053	10:28:39.0	−35:10:53.5	0.096	18.57 (0.10)	1.48 (0.13)	25.8	17.6	24.7	6.8	SE
3	ANTL J102843–353933	10:28:43.8	−35:39:33.1	0.077	18.74 (0.07)	1.76 (0.11)	25.8	14.2	24.8	6.6	SE
4	ANTL J102914–353855	10:29:14.7	−35:38:55.2	0.084	21.35 (0.11)	1.31 (0.14)	25.6	5.1	25.7	2.9	SE, FG
5	ANTL J102918–352900	10:29:18.8	−35:29:00.2	0.090	19.74 (0.01)	1.52 (0.02)	–	9.4	–	–	NS, PHOT
6	ANTL J102932–354216	10:29:32.2	−35:42:16.4	0.084	22.35 (0.08)	1.68 (0.11)	26.5	2.6	25.4	1.6	ELL, PB
7	ANTL J102936–352445	10:29:36.2	−35:24:45.7	0.094	19.00 (0.08)	1.50 (0.11)	25.8	13.0	25.0	6.4	SE, BL
8	ANTL J102943–352238	10:29:43.3	−35:22:38.8	0.098	21.08 (0.04)	1.17 (0.06)	–	9.4	–	–	FG, NG
9	ANTL J102948–352354	10:29:48.6	−35:23:54.0	0.098	22.39 (0.02)	1.90 (0.04)	26.1	2.1	24.5	1.1	ELL, NG
10	ANTL J102954–352744	10:29:54.2	−35:27:44.6	0.094	–	–	–	–	–	–	FG, NS
11	ANTL J102955–351517	10:29:55.9	−35:15:17.6	0.103	18.42 (0.03)	1.70 (0.05)	26.0	9.7	25.3	4.0	ELL, NG
12	ANTL J102959–354227	10:29:59.8	−35:42:27.1	0.089	20.70 (0.03)	1.93 (0.06)	–	10.5	–	–	FG, PHOT
13	ANTL J103027–350957	10:30:27.5	−35:09:57.4	0.101	20.24 (0.04)	1.38 (0.05)	25.9	5.0	25.4	4.4	ELL
14	ANTL J103027–352941	10:30:27.5	−35:29:41.8	0.098	21.24 (0.05)	1.82 (0.09)	–	10.5	–	–	FG, PHOT
15	ANTL J103042–351519	10:30:42.1	−35:15:19.5	0.099	21.02 (0.04)	0.99 (0.06)	–	10.8	–	–	FG, PHOT
16	ANTL J103047–354025	10:30:47.1	−35:40:25.1	0.102	20.37 (0.03)	1.02 (0.04)	–	10.8	–	–	FG, BL, PHOT

Notes. Here, μ_{T_1} corresponds to the threshold above which SExtractor detects and measures the object (MU_THRESHOLD) or to the surface brightness of the outermost isophote for ELLIPSE. r_{T_1} is the radius that contains 90 per cent of the light for SExtractor, the equivalent radius ($r = \sqrt{ab} = a\sqrt{1-\epsilon}$) of the most external isophote for ELLIPSE, or the radius of the aperture considered with PHOT. $\langle\mu_{\text{eff}}\rangle$ is obtained from r_{eff} , the radius that contains one-half of the light (see equation 1 in Paper I). This radius is the output parameter FLUX_RADIUS for SExtractor. Remarks refer to SE = magnitudes and colours measured with SExtractor; ELL = magnitudes and colours obtained with ELLIPSE; PHOT = magnitudes and colours measured with PHOT; BL = bleeding; NS = nearby a bright star; NG = nearby a bright galaxy; FG = very faint and diffuse galaxy and PB = possible background.

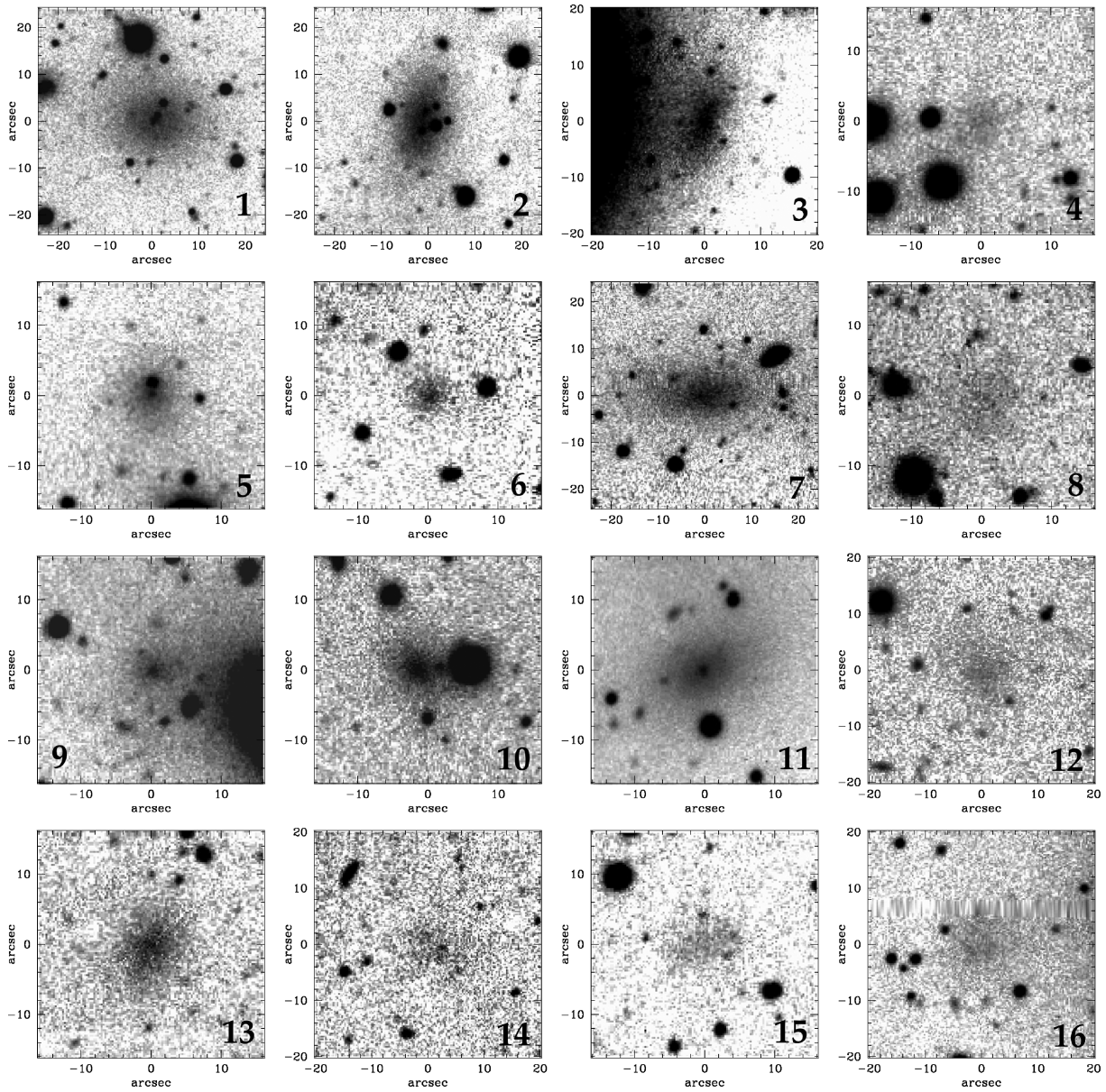


Figure B2. Logarithmic scale R images of the new dwarf galaxy candidates identified in the central region of the Antlia cluster. The number at one of the lower corners corresponds to the number in Table B2. North is up and east is to the left.

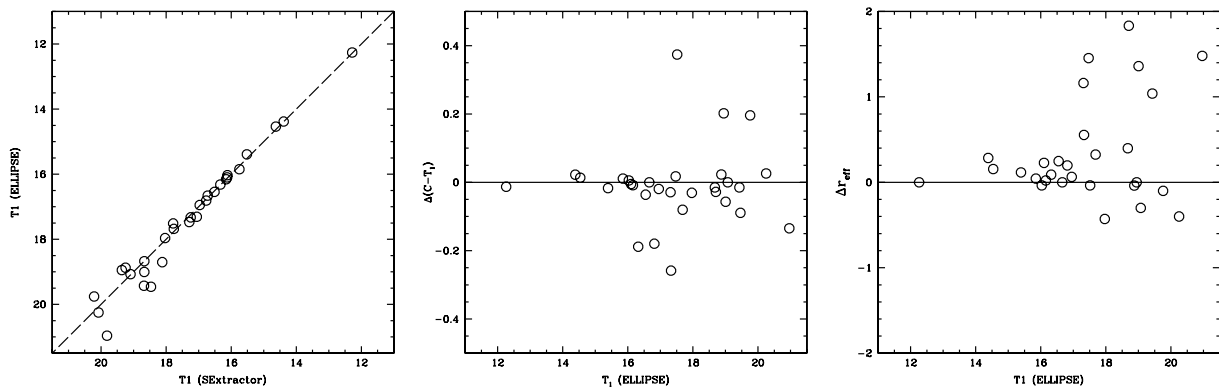


Figure C1. Comparison between T_1 magnitudes (left), $(C - T_1)$ colours (centre) and effective radii (right), obtained with ELLIPSE and SExtractor.

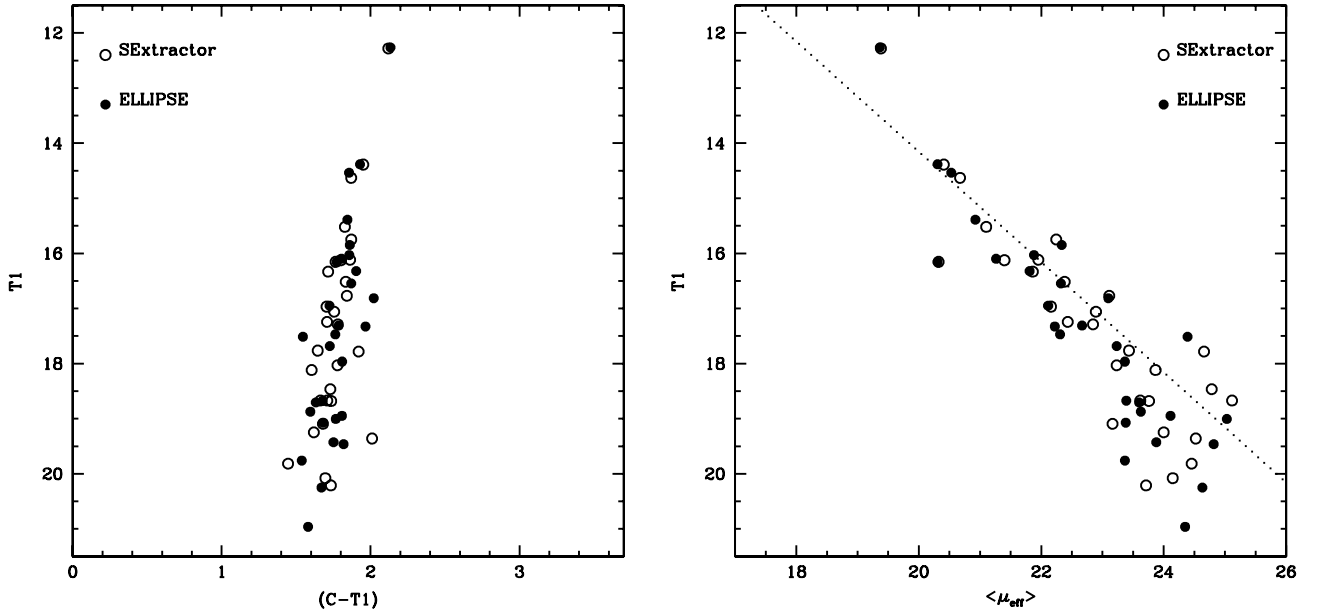


Figure C2. Comparison between colour–magnitude and $\langle\mu_{\text{eff}}\rangle$ –luminosity relations obtained with ELLIPSE and SExtractor.

Table C1. ELLIPSE photometry of FS90 early-type galaxies placed in the central region of Antlia that were presented with SExtractor photometry in Paper I. All the photometric relations analysed in the present paper were built with these values.

FS90 ID	FS90 mor.	FS90 status	T_1 (mag)	$(C - T_1)$ (mag)	μ_{T_1} (mag arcsec $^{-2}$)	r_{T_1} (arcsec)	$\langle\mu_{\text{eff}}\rangle$ (mag arcsec $^{-2}$)	r_{eff} (arcsec)
70	dE	1	17.68 (0.02)	1.73 (0.08)	26.4	12.9	23.2	5.1
72	S0	1	14.38 (0.01)	1.93 (0.02)	26.4	29.7	20.3	6.1
73	dE	1	16.95 (0.01)	1.72 (0.04)	27.0	15.1	22.1	4.3
85	dE	1	18.70 (0.01)	1.63 (0.04)	25.3	6.6	23.6	3.8
87	dE, N	1	15.85 (0.01)	1.86 (0.04)	26.8	23.4	22.3	7.9
114	dE	1	20.96 (0.02)	1.58 (0.05)	26.4	3.6	24.3	1.9
118	dE	1	19.01 (0.03)	1.77 (0.14)	26.5	11.3	25.0	6.4
123	dE, N	2	16.32 (0.01)	1.90 (0.03)	26.4	17.2	21.8	5.0
133	d:E, N	1	14.54 (0.01)	1.86 (0.02)	26.8	29.2	20.5	6.3
136	dE, N	1	16.03 (0.01)	1.86 (0.04)	26.6	21.3	21.9	5.9
159	d:E, N?	1	16.10 (0.01)	1.81 (0.03)	26.7	16.2	21.3	4.3
160	dE	1	19.46 (0.02)	1.82 (0.07)	27.7	9.4	24.8	4.7
162	dE, N	1	17.31 (0.02)	1.78 (0.04)	25.8	11.6	22.7	4.7
176	dE, N	1	17.33 (0.01)	1.97 (0.03)	25.7	10.1	22.2	3.8
177	d:E, N	1	15.39 (0.01)	1.84 (0.03)	26.0	20.0	20.9	5.1
186	dE	1	18.67 (0.02)	1.68 (0.05)	26.0	7.7	23.4	3.5
188	dE	1	17.96 (0.02)	1.81 (0.08)	26.4	11.1	23.4	4.8
192	E(M32?)	3	16.66 (0.01)	2.11 (0.03)	27.6	11.4	19.9	1.7
201	dE	1	19.43 (0.02)	1.75 (0.06)	26.3	6.5	23.9	3.1
216	E	2	16.15 (0.01)	1.77 (0.02)	27.2	13.8	20.3	2.7
228	dE, N	1	17.47 (0.01)	1.76 (0.06)	27.0	13.1	22.3	3.7
231	d:E, N	1	14.97 (0.01)	2.19 (0.02)	26.7	21.7	20.4	4.9
241	dE, N	1	16.81 (0.02)	2.02 (0.08)	26.7	18.8	23.1	7.2

Notes. Here, μ_{T_1} corresponds to the surface brightness of the outermost isophote measured with ELLIPSE. r_{T_1} is the equivalent radius ($r = \sqrt{ab} = a\sqrt{1-\epsilon}$) of the most external isophote. $\langle\mu_{\text{eff}}\rangle$ is obtained from r_{eff} , the radius that contains one-half of the light, following equation (1) of Paper I.

offsets as large as $|\Delta(C - T_1)| = 0.4$ mag might arise for some objects: 6 galaxies out of 30 (20 per cent) present $|\Delta(C - T_1)| > 0.2$ mag.

When effective radii are compared (right panel of Fig. C1), those obtained by SExtractor tend to be larger than those found by ELLIPSE. In the plot, we considered $\Delta r_{\text{eff}} = r_{\text{eff}}^{\text{SEx}} - r_{\text{eff}}^{\text{ELL}}$. In particular,

for $T_1 > 17$ mag, the mean offset is $|\Delta r_{\text{eff}}| = 0.8$ arcsec and for $T_1 < 17$ mag, $|\Delta r_{\text{eff}}| = 0.1$ arcsec.

Despite these differences, we see from both panels of Fig. C2 that our conclusions about the colour–magnitude and luminosity– $\langle\mu_{\text{eff}}\rangle$ relations almost do not change by considering photometry obtained by one way or another. The slope and zero-point of both CMRs are

similar, and the locus of constant effective radius arises naturally in both samples. `SEXTRACTOR` photometry seems to introduce some additional scatter at the faint end of the relation, while `ELLIPSE` slightly increases the dispersion at intermediate brightness. The luminosity– μ_{eff} relation presents lower scatter when the `SEXTRACTOR` photometry is considered. However, the break at the faint end of the relation is found in both samples. In the case of FS90 192, one of the cE galaxies, it can be seen that its location away from the locus of constant effective radius towards higher values of $\langle\mu_{\text{eff}}\rangle$ is similar in both cases.

From our findings we conclude that `SEXTRACTOR` and `ELLIPSE` are suitable to study mean photometric relations with a comparable level of confidence. However, for individual studies of low brightness galaxies, some care must be taken when considering colours and structural parameters.

This paper has been typeset from a `TEX/LATEX` file prepared by the author.